Laser Sensing for Quality Control and Classification – Applications for the Food Industry, Ecology and Medicine

Lundin, Patrik

2014

Total number of authors:
1

Laser Sensing for Quality Control and Classification – Applications for the Food Industry, Ecology and Medicine

Patrik Lundin

Doctoral Thesis
2014

Lund University

LASER SENSING FOR QUALITY CONTROL AND CLASSIFICATION – APPLICATIONS FOR THE FOOD INDUSTRY, ECOLOGY AND MEDICINE

It is easier to see a single, faint star on a cloudy night

Than to count the multitude in a clear sky

Abstract

Monitoring constitutes a cornerstone, both for efficient control of optimized industrial processes and for obtaining knowledge about non-controlled, natural phenomena.

This thesis is all about monitoring, or measurements. In this case the primary information is gathered with light, and in a non-intrusive, and usually a stand-off or remote way.

The applications of optical monitoring in this work are directed towards some main areas: atmospheric gas monitoring, the food industry, ecology, and medicine. Some of the work cannot be classified as belonging solely to one of those groups, but is instead aimed at improving optical monitoring in general.

Monitoring of gases in food packaging is the primary area within the food industry explored in the work of this thesis. A current trend is that food is increasingly often packed in so called modified atmospheres, where the air surrounding the product in the package has been replaced by another gas mixture. Monitoring is currently performed by intrusive spot-checks on a small number of packages, to make sure that they are actually tight enough to maintain the modified atmosphere all the way from manufacturing to the kitchen of the consumer. The studies in this thesis aim at introducing non-intrusive methods based on diode laser absorption spectroscopy, by which the gas in the packages may be checked, and re-checked, without breaking the seal. A long-term goal that could be realized with this technique is that more packages could be checked, perhaps on the production line and, at later stages, in the store. Waste could in this way be reduced if poor packing can be avoided, or remade, and the packing process and materials improved. The results are so far very promising and one specific technique variety was commercialized during the time of this thesis work.

Diode laser spectroscopy has also been used in the medical field, where the primary goal was to introduce a way to monitor the air distribution in the lungs and intestines of prematurely born children. Both of these organs are often affected by a premature birth, and our results indicate that spectroscopic gas monitoring could be helpful. Interestingly enough, the techniques used for these medi-

cal measurements and for the packaging industry applications are almost identical.

Apart from the work related to the food's packaging a pair of studies were also performed on the "food" directly, namely on apple tissue and on tea. In a study of gas exchange in apples it was found, to our surprise, that apple pieces exposed to vacuum could maintain a low internal pressure for hours after re-exposure to ambient pressure. In a study on tea, fluorescence spectroscopy was evaluated as a means to obtain information on the quality of the product with a rapid, stand-off technique. A good correlation was found between the assessment by tea tasting experts and the fluorescence technique.

Fluorescence spectroscopy was also used in this work on other organic materials, in the field of ecology where damselflies and birds were studied with the light detection and ranging (LIDAR) technique. Harmless pulses of UV laser radiation were emitted in a beam out into the atmosphere. The UV radiation induces fluorescence in the feathers of the birds and the abdomen and wings of the damselflies. The spectral features of the fluorescence are characteristic for different species, genders, or other characteristics, of the animals, and the technique can therefore be used for classification. The analogy with the tea study is strong.

Populärvetenskaplig Sammanfattning

Olika mätningar och övervakning utgör viktiga verktyg för kontroll och styrning av optimerade industriprocesser, men också för att få kunskap om naturliga fenomen. I denna avhandling används ljus för att utföra monitorering på ett icke-invasivt vis, ofta till och med genom att studera objekt på avstånd. De områden inom vilka de optiska teknikerna tillämpas i denna avhandling innefattar huvudsakligen förpackningsindustrin, ekologi och medicin.

En gällande trend inom förpackningsindustrin idag är att allt fler produkter förpackas i s.k. modifierade atmosfärer. Det innebär att luften i förpackningen byts ut mot någon annan gasblandning, vanligvis innehållande mycket kväve eller koldioxid. Anledningen är att man vill öka produktens livslängd. För att kontrollera att den nya atmosfären är korrekt, utförs stickprov med gasanalys på ett litet antal förpackningar, vilka därmed förstörs. Denna avhandling innehåller studier med mål att utveckla laserbaserade tekniker för att kunna mäta vilken gasblandning som finns inuti förpackningen utan att öppna den. I detta fall skulle fler (kanske alla) förpackningar kunna kontrolleras, vilket skulle kunna innebära att färre produkter går till spillo, och att förpackningsprocessen kan optimeras ytterligare.

Diodlaserspektroskopi används i denna avhandling också inom det medicinska området, där det långsiktiga målet är att mäta mängden luft, och halten syrgas i lungorna och tarmarna på för tidigt födda barn. Båda dessa organ löper stor risk att påverkas negativt av en för tidig födsel. Att kunna mäta, t.ex., fördelningen av syrehaltig luft i lungorna skulle kunna förbättra den vård som ges i ett tidigt skede efter födseln. Studierna visar lovande resultat medan den kliniska nyttan fortfarande behöver bevisas i kliniska studier.

Utöver det arbete som rör mat*förpackningar*, har en del studier inom avhandlingen handlat om att studera matprodukter i sig, i detta fall äpplen och te. I en studie på äpplen upptäcktes, till vår stora förvåning, att äpplebitar utsatta för vakum kan hålla kvar

det låga trycket i dess porer i flera timmar efter återexponering för normalt tryck. En annan studie handlade om att på ett automatiserat sätt kunna bedöma kvaliteten på torkat te. För detta användes skillnader i fluorescensens spektrum för olika typer av te. Resultaten från mätningarna visade stor överensstämmelse med utfallet från en grupp téexperters smaktester.

Fluorescens användes också för att på avstånd kunna bestämma art och kön hos sländor och fåglar. Harmlösa ljuspulser skickades ut i luften, och när dessa träffar, t.ex., en fågel, skickas fluorescens ut, med en färg som beror på fågelns art. Förhoppningen är att tekniken ska kunna artbestämma fåglar och insekter på ett automatiserat sätt, och på stort avstånd. Detta kan få stor betydelse för att bättre förstå hur fåglar flyttar, inte minst på natten, och hur sländor migrerar i naturen.

LIST OF PUBLICATIONS

This thesis is based on the following papers, which will be referred to by their Roman numerals in the text.

I **Active feedback regulation of a Michelson interferometer to achieve zero-background absorption measurements**
P. Lundin, Z.G. Guan, and S. Svanberg.
Applied Optics **50**, 373–378 (2011).

II **Vertical lidar sounding of atomic mercury and nitric oxide in a major Chinese city**
Z.G. Guan, P. Lundin, L. Mei, G. Somesfalean, and S. Svanberg.
Applied Physics B **101**, 465–470 (2010).

III **First attempt to monitor atmospheric glyoxal using differential absorption lidar**
L. Mei, P. Lundin, G. Somesfalean, J. Hu, G. Zhao, S. Svanberg, J. Bood, M. Vrekoussis, and A. Papayannis.
Proc. SPIE **8534**, 853412-1–853412-6 (2012).

IV **Non-intrusive measurements of headspace gas composition in liquid food packages made of translucent materials**
M. Lewander, P. Lundin, T. Svensson, S. Svanberg, and A. Olsson.
Packaging Technology and Science **24**, 271–280 (2011).

V **Non-intrusive headspace gas measurements by laser spectroscopy – Performance validation by a reference sensor**
P. Lundin, L. Cocola, M. Lewander, A. Olsson, and S. Svanberg.
Journal of Food Engineering **111**, 612–617 (2012).

VI **Assessment of photon migration in scattering media using heterodyning techniques with a frequency modulated diode laser**
Z.G. Guan, P. Lundin, and S. Svanberg.
Optics Express **17**, 16291–16299 (2009).

VII **Gas spectroscopy and optical path-length assessment in scattering media using a frequency-modulated continuous-wave diode laser**
L. Mei, H. Jayaweera, P. Lundin, S. Svanberg, and G. Somesfalean.
Optics Letters **36**, 3036–3038 (2011).

VIII **Characterization and validation of the frequency-modulated continuous-wave technique for assessment of photon migration in solid scattering media**
L. Mei, P. Lundin, S. Andersson-Engels, S. Svanberg, and G. Somesfalean.
Applied Physics B **109**, 467–475 (2012).

IX **Laser spectroscopic gas concentration measurements in situations with unknown optical path length enabled by absorption line shape analysis**
P. Lundin, L. Mei, S. Andersson-Engels, and S. Svanberg.
Applied Physics Letters **103**, 034105-1–034105-4 (2013).

X **Diffuse optical techniques applied to wood characterisation**
I. Bargigia, A. Nevin, A. Farina, A. Pifferi, C. D'Andrea, M. Karlsson, P. Lundin, G. Somesfalean, and S. Svanberg.
Journal of Near Infrared Spectroscopy **21**, 259–268 (2013).

XI **Gas in scattering media absorption spectroscopy (GASMAS) detected persistent vacuum in apple tissue after vacuum impregnation**
U. Tylewicz, P. Lundin, L. Cocola, K. Dymek, P. Rocculi, S. Svanberg, P. Dejmek, and F. Gómez Galindo.
Food Biophysics **7**, 28–34 (2012).

XII **Tea classification and quality assessment using laser-induced fluorescence and chemometric evaluation**
L. Mei, P. Lundin, M. Brydegaard, S. Gong, D. Tang, G. Somesfalean, S. He, and S. Svanberg.
Applied Optics **51**, 803–811 (2012).

XIII **Insect monitoring with fluorescence lidar techniques: field experiments**
Z.G. Guan, M. Brydegaard, P. Lundin, M. Wellenreuther, A. Runemark, E.I. Svensson, and S. Svanberg.
Applied Optics **49**, 5133–5142 (2010).

XIV **Feasibility study: fluorescence lidar for remote bird classification**
M. Brydegaard, P. Lundin, Z.G. Guan, A. Runemark, S. Åkesson, and S. Svanberg.
Applied Optics **49**, 4531–4544 (2010).

XV **Remote nocturnal bird classification by spectroscopy in extended wavelength ranges**
P. Lundin, P. Samuelsson, S. Svanberg, A. Runemark S. Åkesson, and M. Brydegaard.
Applied Optics **50**, 3396–3411 (2011).

XVI **Passive unmanned sky spectroscopy for remote bird classification**
P. Lundin, M. Brydegaard, L. Cocola, A. Runemark, S. Åkesson, and S. Svanberg.
Proc. SPIE **8174**, 81740-J-1–81740-J-11 (2011).

XVII **Noninvasive monitoring of gas in the lungs and intestines of newborn infants using diode lasers: feasibility study**
P. Lundin, E. Krite Svanberg, L. Cocola, M. Lewander Xu, G. Somesfalean, S. Andersson-Engels, J. Jahr, V. Fellman, K. Svanberg, and S. Svanberg.
Journal of Biomedical Optics **18**, 127005-1–127005-8 (2013).

Abbreviations

BFO	Beat frequency oscillator
DAQ	Data acquisition card
DFB	Distributed feedback
FMS	Frequency modulation spectroscopy
FSR	Free spectral range
MRI	Magnetic resonance imaging
FDPM	Frequency-domain photon migration
FMCW	Frequency-modulated continuous wave
FMLSI	Frequency-modulated light scattering interferometry
FMS	Frequency modulation spectroscopy
GASMAS	Gas in scattering media absorption spectroscopy
KETs	Key enabling technologies
laser	Light amplification by stimulated emission of radiation
LIDAR	Light detection and ranging
LIF	Laser-induced fluorescence
MAP	Modified atmosphere packaging
MTOF	Mean time-of-flight
NEC	Necrotizing enterocolitis
NICU	Neonatal intensive care unit
PC	Principal component
PCA	Principal component analysis
PD	Photo-diode
PMT	Photomultiplier tube
RDS	Respiratory distress syndrome
TCSPC	Time-correlated single photon counting
TDLAS	Tunable diode laser absorption spectroscopy
TIA	Transimpedance amplifier

TOF	Time-of-flight
TOFS	Time-of-flight spectroscopy
TRS	Time resolved spectroscopy
RF	Radio frequency
US	Ultrasonography
VOC	Volatile organic compound
WMS	Wavelength modulation spectroscopy

Contents

Papers

Introduction

In 2009 the European Commission announced five so-called "Key Enabling Technologies", KETs, which were regarded as the technologies with the greatest potential to solve societal challenges. Photonics was, and still is, on that list, together with nanotechnology, micro- and nano-electronics, advanced materials, and biotechnology [1]. The description of photonics given in the report by the European Commission was "Photonics is a multidisciplinary domain dealing with light, encompassing its generation, detection and management. Among other things it provides the technological basis for the economical conversion of sunlight to electricity which is important for the production of renewable energy, and a variety of electronic components and equipment such as photodiodes, LEDs and lasers". As seen there, and elsewhere, photonics deals with creating, handling and detecting light in clever ways. Although the conversion of sunlight into electricity is not discussed in this thesis, the presented work has dealt very much with lasers and the light they generate, with various components to handle the light, and with using photo-diodes (which, in fact, are very similar to solar panels) to detect light.

It would be wonderful to be able to say that the work presented has actually also contributed to "solve societal challenges". Such complementary words are clearly not motivated by this work alone, but hopefully some pieces have been added to the huge jigsaw puzzle of technologies and knowledge that could possibly do so. It is probably safe to say that the aim of all the studies presented is to push developments in that direction. Some overall, long-term goals of the work can be mentioned: reducing unnecessary use of antibiotics, reducing spoilage of food, and contributing to a better understanding of atmospheric physics and chemistry. The work has, of course, been trying to make small improvements and find answers to more specific questions.

1.1   Structure of the thesis

The work included in this thesis has consisted of developing and improving spectroscopic monitoring techniques. These techniques could have a large number of applications but the few we have focused on are introduced in Chap. 2 – "Background". The purpose there is to give a short background to the applications and to explain why these areas are important to study, and how our measured parameters could be of use. The applications introduced here include environmental monitoring of the atmosphere; food safety; remote sensing in animal ecology; and gas sensing in infant lungs and intestines. Although the applications may seem quite diverse, the techniques used in the studies are actually very similar, pointing to the broad inter-disciplinarity of the work.

The following chapter, Chap. 3 – "Concepts for optical spectroscopy", describes the basic concepts and physical phenomena behind the parameters used for the measurements in the thesis work. Examples of concepts discussed are light absorption by gases, and fluorescence.

The next chapter, Chap. 4 – "Basic techniques for optical spectroscopy", then introduces the basic techniques that our specialized monitoring methods rely upon. The techniques described here are based on probing parameters related to the physics presented in Chap. 3.

Chap. 5 – "Gas sensing in scattering media" moves closer to the research in the thesis by describing some aspects of the technique "gas in scattering media absorption spectroscopy" (GASMAS). The technique is based on the methods introduced in Sect. 4.1.

Chap. 6 – "Fluorescence light detection and ranging for animal ecology applications" combines the basic concept of fluorescence and the technique "light detection and ranging" (LIDAR, Sect. 4.3). This combination in itself is far from new, but its application to ecological fields presented in Sect. 2 are all the more novel.

Finally, in Chap. 7 – "Conclusion and perspectives", the work is put into context by discussing its relevance and impact.

BACKGROUND

This chapter is devoted to giving a short background to the major application areas addressed in this thesis. A broad background to the applications and how our techniques and approaches can become useful to them are presented.

The reader might be surprised by the diversity of the applications in this thesis. A small comment on this, at the outset, is therefore probably reasonable. Despite the very different application fields, the technical backgrounds and challenges are very similar. For the applications addressing environmental monitoring of the atmosphere (Sect. 2.1, Papers **II** and **III**), the technique differential absorption LIDAR (DIAL), measuring atmospheric gas absorption was employed. Laser-based gas absorption measurements were also performed in the work regarding food and food safety (Sect. 2.2, Papers **IV**, **V** and **XI**) and in the medical work (Sects 2.4 and 2.5, Paper **XVII**). The technique used here, GAS-MAS, shares many similarities with DIAL, as is specifically discussed in Ref. [2]. Technical developments for general laser-based gas sensing are presented in Papers **I**, and methodological improvements of GASMAS are discussed in Papers **VI**, **VII**, **VIII** and **IX**, and a further application in **X**. The technological platform for atmospheric monitoring with LIDAR (Papers **II** and **III**), was also used for the studies regarding animal ecology (Sect. 2.3, Papers **XIII**, **XIV** and **XV**), although fluorescence was used instead of gas absorption. Fluorescence was also the property studied in Paper **XII**, with the only major difference being that the measurements were performed from a shorter distance.

2.1 Environmental monitoring of the atmosphere

Problems and challenges related to our environment have many facets. Today, most issues are related to our exploitation of natural resources. One corner stone in dealing with these environmental questions, is to characterize the actual status of, e.g., the atmosphere [3], oceans, etc. [4]. For this, quantitative measurements of different parameters need to be performed. Regarding the atmosphere, a number of parameters are repeatedly measured across the world, including aerosol distribution and composition, and the concentrations of trace gases. Although many of the aerosols are of natural origin (such as volcanic, salt, or sand dust), there are also anthropogenic sources, mainly arising from combustion processes [5, 6].

Trace gases include a wide range of gases (all with concentrations below 1% by volume). Again, these have both natural and anthropogenic origins [7]. Many of the gases are considered to be pollutants (e.g., NO, NO$_2$, SO$_2$, Hg,...) and monitoring their distributions is of great importance for formulating the correct interventions.

A major source for nitrogen oxides (NO$_x$) is emissions by engines powered by fossils fuels (mainly car engines) and these have therefore become a major problem in large cities [8, 9]. Mercury (Hg) is present only at very low concentrations in the atmosphere, with background concentrations around 2 ng/m^3. In large cities the concentrations can, however, be much higher, which is a problem due to the toxicity of mercury in general but especially of methylmercury ([CH$_3$Hg]$^+$) which can be formed from atomic mercury in the atmosphere [10]. Glyoxal (C$_2$H$_2$O$_2$) is a trace gas which mainly originates from the oxygenation (for example by OH, O$_3$ or NO$_3$) of hydrocarbons with two or more carbon atoms. The initial formation usually starts from volatile organic compounds like isoprene, which, for example, are emitted by plants. Anthropogenically created initial components also exist, such as acetylene [11, 12].

In this thesis, a variety of the LIDAR technique was applied, trying to measure the concentrations of atomic Hg, NO, NO$_2$ and C$_2$H$_2$O$_2$ in the atmosphere. These studies are found in Papers **II** and **III**.

2.2 Food safety and characterization

Previously very common methods of preserving food, such as salt-curing meat, have today decreased in their popularity, as have frozen products. The general trend is that consumers in the Western World instead desire fresh food to a greater extent. Today,

fresh food is expected to come even from the other side of the globe. This fact has put demands on such things as the transport logistics, as well as on food packages. Packaging is, for many product types, crucial for maintaining food quality as well as for prolonging its shelf-life. As the logistics of transportation and storage must account for keeping, for example, the temperature just right, the package must often account for factors such as maintaining the correct humidity, or avoiding light exposure of the product. Another factor which often is of great importance is to have a suitable gas composition around the product. Although the importance of, e.g., keeping air out of a jar of Sauerkraut, is not exactly news, the method of actively changing the gas composition in food packages has increased in popularity lately.

2.2.1 Modified atmosphere packaging

Like vacuum-packing, modified atmosphere packaging (MAP) is a much employed method for increasing product shelf-life [13]. The method is based on exchanging the air in the headspace of the package for another gas composition. The most common goal of MAP is to reduce the amount of oxygen, which is well known to deteriorate most products. The oxygen is then generally replaced by increasing the concentrations of nitrogen and/or carbon dioxide [14]. As early as 1927 it was shown how the shelf-life of apples was increased by storing them in conditions with a decreased oxygen concentration and increased carbon dioxide [15]. In the 1970's the number of products packaged and transported with modified atmospheres (MAs) increased rapidly, including meat. In seeming contradiction, there is also a trend in some countries to pack meat in high oxygen concentrations to keep the myoglobin in its oxygenated form, giving a "fresh", red appearance, desired by the consumer [14].

With the expanding number of product types packed with MAP, the need for verifying the quality of the MA has increased too. A frequently employed method is to perform spot-checks where needles are used to extract a portion of the head-space gas and perform subsequent gas analysis by electrochemical, IR spectroscopic or mass-spectroscopic means. Since these methods are intrusive, it is very desirable to develop methods that can measure the gas concentrations non-intrusively, even for non-transparent packages. In this way, more products could be examined without waste, which could improve product safety and help to optimize the packing process. Further, studies can be performed where the same package is tested continuously or repeatedly for prolonged time-periods.

Optical techniques often have the property of being non-intrusive, fast, and species selective, and could thus be suitable for this task [16]. This thesis contains studies (Papers **IV**, **V** and

IX) where GASMAS (Sect. 5) is applied to measure gas concentrations in non-transparent food packages.

2.3 Remote sensing in animal ecology

A general desire in the field of animal ecology is to study the behavior of animals without disturbing them. On the other hand, detailed information is hard to collect without being close; often even capture of the animal is needed for studying it, or for ring-marking, applying data loggers, and so on. An appealing alternative is to perform remote sensing, meaning that information is often gathered with no or very little disturbance for the animal, which in turn means that the data collected is a better representation of its natural behavior. Undoubtedly, the most common remote sensing methods are, of course, to observe the animal with the naked eye, with a pair of binoculars, or with a telescope. However, there is much more information to be found in the optical regime, as well as in other parts of the electromagnetic spectrum. In the work of this thesis, remote sensing methods using lasers and IR cameras have been developed to extend and improve the possibilities for remote sensing within animal ecology. The physical phenomenon utilized, fluorescence, is discussed in Sect. 3.2, the general measurement technique in Sect. 4.3, and some of the specific setups and approaches in Chap. 6. The animals studied were damselflies and birds, and they are discussed in more detail in the following subsections.

2.3.1 Remote sensing of damselflies

Studying insect distributions and migration is important not only to learn about the specific insect itself, but also because it permits other factors affecting the animals to be studied indirectly. For example, when observing insects as indicators for a general biological condition, this is generally referred to as using biomarkers or biological markers. A good example is the fact that insects are generally ectotherms so they are highly sensitive to the ambient temperature. The global distribution of a specific species is thus an indicator for long-term temperature changes. In fact, a northward shift of the populations of species on the northern part of the Earth due to global warming has been observed [17]. Another example is damselfly larvae, which are sensitive to water pollutants and the amount of dissolved oxygen in the water. Corresponding information about the water quality can thus be obtained by studying the damselfly population distribution [18].

A commonly employed method for studying the migration of damselflies (and other insects) is to capture individuals from a certain population, and to mark them, for example with a colored

powder. A certain time afterward, the spread of these individuals into neighboring habitats is studied. However, this approach is very time consuming as an initial capture, and then also re-capture, are needed.

In the work of this thesis, methods were developed with the aim to classify damselflies regarding gender and species in a remote fashion. The classification is based both on the natural fluorescence signature of the insects, as well as on that of the colored powders traditionally used for marking. The latter approach eliminates the need for a second capture, and provides better statistical information. The study regarding damselflies is found in Paper **XIII**, and an introduction to our approach is found in Sect. 6.1.

2.3.2 Remote sensing of bird migration

The highly evolved physiology of birds has enabled successful colonization of most geographical locations on the Earth [19], as well as adaptation to rather extreme migratory flights. During their long-distance migrations, birds cross deserts and seas, for instance to spend part of the year in northern Europe and part of the year in Africa [20, 21].

Information about the flight patterns of different species is important for learning about how physiological adaptations and differences affect choices of timing and routes for migration. The effect of weather conditions, as well as changes in major land marks, vegetation spread, and so on, can also be understood from changes in migratory paths.

Further, due to the bird's high mobility, they make a large contribution to the spread of diseases, such as avian flu and avian malaria, as well as to the spread of other things, such as seeds. Insight into migration flights can thus also improve our understanding of how, e.g., diseases are spread [21], and could even help us predict and possibly prepare for major outbreaks.

It is today very difficult to perform remote species classification for a large proportion of the migrations. Many birds migrate during the night (nocturnally) [22], even the majority of song birds do so. At night, the air is generally less turbulent [23], the predation rate is lower [24], and the birds can use the daytime for foraging. Further, migration often occurs at high altitudes, above 500 m.

Radar is frequently used for remote bird studies, thanks to the ability of radars to monitor flight directions and altitudes, as well as the number of birds passing [25]. The strength of the echo, together with the wing beat frequency (which modulates the echo strength), can also be used for a crude size classification. However, a more detailed classification is generally hard to achieve.

To improve the possibilities for remote bird classification, a part of the work of this thesis was devoted to development of laser-based, and of passive sensing suitable for monitoring flying birds.

Sect. 6.2 discusses some of the approaches used in this thesis, and the specific studies involving birds are found in Papers **XIV**, **XV** and **XVI**.

2.4   Gas monitoring in infant lungs

A preterm birth increases the risk of complications since many of the infant's organs are immature. The lungs are among the last organs to mature during pregnancy which means that these are often affected by a preterm birth. One of the severe conditions that can strike a baby is Respiratory distress syndrome (RDS). This is a condition with an uneven distribution of gases in the lungs, and both overinflated and collapsed parts exist. The risk of decreased oxygen uptake is therefore large. The main organ at risk of injury due to insufficient oxygen delivery is the brain [26–28]. The cause of RDS is immature lungs where there is an insufficient production of the surfactant coating the inside of the alveoli. The symptoms of RDS usually appear directly after birth and include a fast breathing rate, an increased heart rate, chest wall retractions, or cyanosis.

It is very important to diagnose RDS quickly and to provide respiration assistance as the morbidity is otherwise increased with a potential for chronic lung disease and brain damage. Although, e.g., pulse oximetry can give data for the overall oxygen uptake, it does not provide information about the cause. Today, the main diagnostic method for RDS is X-ray scanning, which, as is well known, can be harmful, especially for infants, and on repeated exposure. Ultrasonography (US) provides a quite harmless diagnosis alternative to X-rays. The technique could be used to map out the lungs, being air-filled spaces within the body. A drawback of US is that it does not provide any information about the constituents of the gas (oxygen, nitrogen or carbon dioxide), something which is important for a correct diagnosis, especially when assessing the severity of the disease.

Diagnosis and monitoring of the treatment progress would be improved with a minimally invasive technique capable of measuring the spatial gas distribution and gas constituents within the lungs.

Paper **XVII** presents the first *in vivo* measurements using the GASMAS technique (Sect. 5) for detection of free gas in the lungs of three infants. The study is hopefully a step towards a non-intrusive way to monitor the gas in the lungs of preterm infants. The goal is that the GASMAS technique should assist doctors in the diagnosis, treatment and follow-up of respiratory distress syndrome.

2.5 Gas monitoring in infant intestines

Another problem area for prematurely born infants is that the stomach and the intestine are at risk of being underdeveloped. The second most common cause of morbidity of premature infants is Necrotizing enterocolitis (NEC) [29], which strikes between 1% and 8% of all newborns at a neonatal intensive care unit, and 90% of those cases occur among preterm infants [30]. NEC is an inflammatory disease in which parts of the intestine experience necrosis (tissue death). The walls of the intestine become thinner and there is also risk of intestinal perforation, leading to severe complications with high morbidity and mortality rates [31]. The amount of gas in the intestine increases, leading to abdominal distension. Other early symptoms are intolerance to feeding, increased gastric residuals, and bloody stools. If the intestine is completely perforated, food and bacteria can pass through and acute complications therefore include sepsis (blood poisoning), wound infections and localized formation of pus surrounded by inflamed tissue. Long term complications include intestinal strictures and short gut [32].

The gas related symptoms of NEC make it natural to use the GASMAS technique for detection, and this aspect is discussed in Paper **XVII**.

Concepts for optical spectroscopy

The aim of this chapter is to provide a background to the underlying concepts for the spectroscopic methods used in the thesis work. Gaseous light absorption is essential for most of the studies presented and therefore form a major part of this chapter. Apart from this, fluorescence is also a key phenomenon relevant to this work, and is thus introduced briefly here.

3.1 Some physics of light absorption by gases

It is a well known fact that solid and liquid matter generally absorb light in quite broad spectral features, while gases absorb in very narrow spectral " lines". This general behavior is sketched in Fig. 3.1 where the broad absorption features of red wine only transmit the red part of the spectrum, while the very narrow absorption lines of a gas are generally too limited to create imprints noticeable to human color vision. As a consequence, most gases are colorless. This fundamental difference between light absorption by gases and solid or liquid matter is one of the cornerstones of the GASMAS technique (Chap. 5) used in many of the papers of this thesis.

This section will present some of the physics of light absorption by gases, and the parameters which affect the shape of gaseous absorption lines. This subject is of underlying importance in many of the papers and is especially central in Paper **IX**. The chapter starts with some basic knowledge about the energy level structure of molecules.

Figure 3.1. *The difference between light absorption by solid or liquid matter and by gases.*

Figure 3.2. *Schematic energy level diagram of a diatomic molecule. The top diagram shows the two lowest electronic energy levels. The dotted box is enlarged into the middle diagram, showing the vibrational levels of the lower electronic level. This dotted box is in turn enlarged into the bottom figure showing the rotational levels of the lowest vibrational level. The spacing between these lines is approximately quadratic in behavior as given by Eq. (3.3).*

3.1.1 Energy level structure of molecules

When molecules are disturbed by surrounding matter to only a small extent, the possible energies they can have are quantized. In short, the energy levels of a free molecule are divided into "electronic", "vibrational" and "rotational" ones; see Fig. 3.2 for a schematic example in the diatomic case. The electronic energy levels describe the energy of the molecule for different configurations of the electrons, similarly to the case for atoms, with the difference now that for molecules these energies are also functions of the distances between the atoms constituting the molecule. For the diatomic case, the electronic energy of the molecule is a function of the distance between the two atoms – the inter-atomic distance. The two lowest electronic levels are drawn in Fig. 3.2 according to the Morse potential, given by Eq. (3.1), with minima for certain atomic separations, an energy going toward a constant value for larger separations, and a value quickly approaching infinity for very short separations.

$$E_{\mathrm{elec}}(r) = E_{\mathrm{min}} + E_{\mathrm{diss}} \left(1 - e^{-a(r-r_{\mathrm{e}})} \right)^2 \qquad (3.1)$$

Here, E_{min} is the energy at the bottom of the well, E_{diss} is the dissociation energy (which is defined from the absolute bottom of the parabola, meaning that it is slightly larger than the true

Unit	Electronic	Vibration	Rotation
cm^{-1}	30000	1000	10
eV	4	0.1	0.001
J	6×10^{-19}	2×10^{-20}	2×10^{-22}

Table 3.1: Approximate contributions for the different parts of the molecular energy.

dissociation energy), a is a constant affecting the width of the well, and r_e is the equilibrium bond distance. The value at large separations is simply the sum of the energies of the two atoms (or ions) when they are not part of a molecule.

For each electronic configuration the atoms will vibrate around r_e with a certain amplitude and frequency, this also in quantized steps. Included in Fig. 3.2 are also symmetric, second degree polynomial parabolas which can approximate the Morse potentials close to the bottom of the well. An approximate equation for the vibrational energy for the diatomic case is given by Eq. (3.2) [33].

$$E_\text{vib} = h\nu_0 \left((v + \frac{1}{2}) - x_\text{e}(v + \frac{1}{2})^2 \right) \tag{3.2}$$

Here, ν_0 is the basic vibrational frequency of the molecule (ν will later be used for optical frequency), $v = 0, 1, 2, ...$ is the vibrational quantum number, h is Planck's constant and x_e is the anharmonicity constant.[1] This vibration adds kinetic energy to the molecule, giving rise to the gray lines seen in the top and middle part of Fig. 3.2. Every vibrational level is then, in turn, composed by a number of rotational energy levels – for each electronic configuration, for each vibrational state, the molecule can also rotate with a number of speeds and directions. This rotation also adds kinetic energy, described approximately for the diatomic case as

$$E_\text{rot} = BJ(J+1) - DJ^2(J+1)^2,$$
$$B = \frac{\hbar^2}{2\mu r_0{}^2}, \quad D = B^3/(\nu_0\pi)^2. \tag{3.3}$$

Here, $\hbar$ is the reduced Planck's constant, μ is the reduced mass of the molecule, r_0 is the inter atomic distance, and $J = 0, 1, 2, ...$ is the rotational quantum number. The total molecular energy becomes $E_\text{tot} = E_\text{elec} + E_\text{vib} + E_\text{rot}$, where examples of some typical values for the different energy contributions are shown in Table 3.1 in different units.

[1] The anharmonicity term forms the major difference between the results of using the second degree polynomial parabola and the Morse potential.
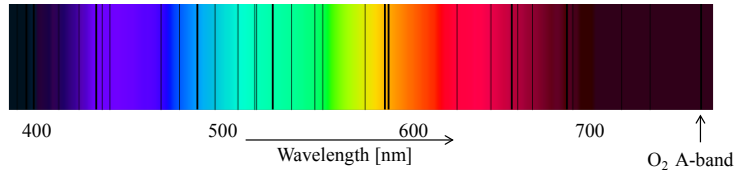
Figure 3.3. *Some of the Fraunhofer lines in the solar spectrum. These absorption lines are due to absorption in the solar atmosphere or in the Earth's atmosphere (terrestrial lines) [34].*

3.1.2   Absorption lines

The well-known spectral emission and absorption lines related to free molecules in gases arise due to transitions between the energy levels just described. A molecule having two levels with energies E_1 and E_2 can, if it initially has the energy E_1, absorb radiation matching the energy difference between these two levels, and is thereby excited to the level E_2. A prerequisite is that the transition between these two levels is quantum mechanically allowed – a subject of its own which is not discussed in this thesis. The light must have a frequency (approximately, as will be discussed later) given by $\nu = (E_2 - E_1)/h$. On the other hand, when the molecule is in the excited state with energy E_2, it can release the extra energy $E_2 - E_1$, by emitting light with the frequency ν. Seen in the spectral domain, the molecule has a spectral line – either an absorption line or an emission line, depending on the process – at the spectral position with frequency ν, corresponding to a wavelength $\lambda = c/\nu$. The well-known Fraunhofer lines in the solar spectrum, seen in Fig. 3.3, are good examples of the absorption case. Most of the lines in this spectrum are due to atoms and ions in the solar atmosphere; however, the indicated lines at around 760 nm (hardly visible) belong to the molecular oxygen A-band. These lines are much used for oxygen sensing in this thesis work, as will be discussed in Chap. 5.

3.1.3   Line shapes and broadening

Spectral lines are never infinitely narrow, no matter how good the performance of the spectrometer. The absorption related to a molecular transition is always distributed around a central wavelength or frequency. The width and shape of this distribution is dependent on the molecule and its surrounding conditions.

Natural (inherent) linewidth

The most fundamental reason for the finite line width is natural broadening. The limited lifetime of the atomic and molecular energy levels gives rise to an uncertainty in their energy. This inexact energy can be related to the fundamental quantum mechanical uncertainties which exist, for example between time and energy, in that a wave packet with a limited time duration cannot be perfectly defined in energy. A Fourier based analysis can also be used, where the Fourier transform of a damped oscillation with an envelope as an exponential decay is applied.

One way to implement a general broadening mechanism is to use a so called autocorrelation function, $\Phi(t)$ [35]. The lineshape is then obtained through the Fourier transform of this function, including the complex representation of the wave oscillating with frequency, ν_0; see Eq. (3.4).

$$\chi(\nu) \propto \left| \mathrm{Re} \left\{ \int_0^\infty \Phi(t) \exp(-2\pi i \nu t) dt \right\} \right|^2 \qquad (3.4)$$

In the case of the natural broadening, $\Phi(t)$ represents the single-exponential decay resulting from a state with lifetime τ.

$$\Phi_\mathrm{N}(t) = \exp((-1/(2\tau) + 2\pi i \nu_0)t) \qquad (3.5)$$

Fig. 3.4 shows an example with a damped oscillation with intensity falling with an exponential time constant, $\tau = 0.5$ ns, and the corresponding spectral intensity distribution to the right. Calculating the FWHM of the intensity distribution gives

$$\Delta\nu = 1/(2\pi\tau), \quad \Delta E = \hbar/\tau. \qquad (3.6)$$

Consider now that the energy levels E_1 and E_2 have associated lifetimes τ_1 and τ_2 (where the excited level has the shortest lifetime). The levels thus experience uncertainties in energy given by

$$\Delta E_1 = \hbar/\tau_1, \ \Delta E_2 = \hbar/\tau_2. \qquad (3.7)$$

In a transition between these two levels, both their energy uncertainties contribute, as seen in Fig. 3.5, giving

$$\Delta E = \sqrt{\Delta E_1{}^2 + \Delta E_2{}^2} = \hbar\sqrt{1/\tau_1{}^2 + 1/\tau_2{}^2}. \qquad (3.8)$$

Conversion to frequency gives

$$\Delta\nu = \Delta E/h = \frac{1}{2\pi}\sqrt{1/\tau_1{}^2 + 1/\tau_2{}^2}. \qquad (3.9)$$

The shape of the naturally broadened line, derived from Eq. (3.5), can now be expressed by the simple relation in Eq. (3.10), and is a Lorentzian profile.
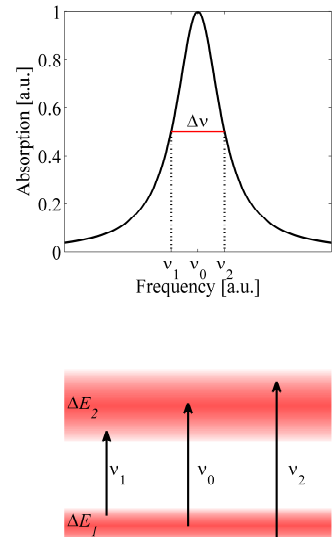
Figure 3.5. *The width of a spectral line and its relation to the "fuzzy" distribution of possible energies of the molecule.*
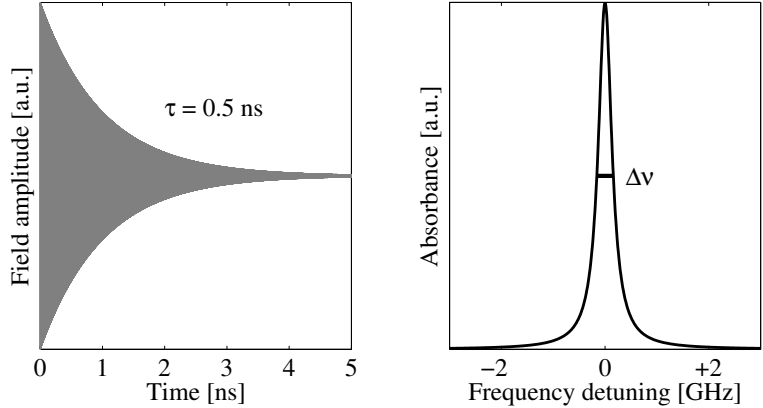
Figure 3.4. *The Lorentzian line shape of a naturally broadened line (right) can be obtained from the (square of the) Fourier transform of a damped oscillation (left). As τ is the decay time for the intensity, the field amplitude reaches $1/e$ at $t = 2\tau$. Note that the gray area consists of an oscillation too fast to be resolved in the figure.*

$$\chi_{\mathrm{N}}(\nu - \nu_0) \propto \frac{1}{(\nu - \nu_0)^2 + (\Delta\nu/2)^2} \qquad (3.10)$$

The natural linewidth is, however, seldom observed in practice as it is concealed by other broadening effects, as is discussed in the following sections.

For a thorough discussion of natural linewidths, please refer to Refs [36] or [37].

Doppler broadening

The thermal motion of atoms and molecules gives rise to further broadening of the absorption and emission lines. This is due to the Doppler effect when the moving molecules encounter the electromagnetic light wave. A molecule traveling towards a wave will experience an increased frequency, and a molecule traveling away, a reduced one. The Doppler shift for any wave with frequency ν_0, and speed c, encountering a molecule with speed v, is given by

$$\nu = \nu_0(1 - v/c \times \cos(\theta)). \qquad (3.11)$$

Here, θ is the angle between the velocity directions of the wave and particle.

The Maxwell-Boltzmann distribution for the speed of molecules in a gas is given by

$$P(v) = 4\pi \left(\frac{m}{2\pi k_{\mathrm{B}} T} \right)^{3/2} v^2 \, \exp\left(-\frac{mv^2}{2k_{\mathrm{B}} T} \right). \tag{3.12}$$

Here, $P(v)$ is the probability distribution of molecular speeds, m is the molecular mass, k_{B} is Boltzmann's constant and T is the absolute temperature. The speed, v, is distributed in all directions, but if only the component along $\mathbf{x}$ is considered, Eq. (3.13) results.

$$P(v_x) = \sqrt{\frac{m}{2\pi k_{\mathrm{B}} T}} \, \exp\left(-\frac{mv_x^2}{2k_{\mathrm{B}} T} \right) \tag{3.13}$$

The first factor is irrelevant when discussing the influence on line broadening, but the second factor sets the shape of the broadening function. Assuming the light goes in the direction $\mathbf{x}$ and encounters a molecule with speed v_x in the same direction, Eq. (3.14) is obtained.

$$\nu = \nu_0 \left(1 - v_x/c \right) \Leftrightarrow v_x = (\nu_0 - \nu)c/\nu_0 \tag{3.14}$$

The probability distribution for the absorbing frequency is now obtained by inserting this expression for the speed into the shape part of Eq. (3.12).

$$P(\nu) \propto \, \exp\left(-\frac{m\left(\frac{\nu_0 - \nu}{\nu_0} c \right)^2}{2k_{\mathrm{B}} T} \right) \tag{3.15}$$

This probability distribution can be seen directly as the intensity distribution of a Doppler broadened spectral line. The FWHM of a Doppler broadened line is given by

$$\Delta \nu_{\mathrm{D}} = \left(\frac{\nu_0}{c} \right) 2\sqrt{2k_{\mathrm{B}} T \ln 2/m}. \tag{3.16}$$

Although the calculation of the Doppler lineshape was performed without explicit use of an autocorrelation function, Φ_{D} (the Doppler autocorrelation function to be used in Eq. (3.4)) is included here for completeness.

$$\Phi_{\mathrm{D}}(t) = \exp\left[-\left(\frac{v_{\mathrm{A}} t}{2\lambda} \right)^2 + 2\pi i \nu_0 t \right] \tag{3.17}$$

Here λ is the light wavelength and v_{A} is the average thermal speed of the probed molecule, given by $v_{\mathrm{A}} = \sqrt{2k_{\mathrm{B}} T/m}$.

Collisional broadening

Another very important line broadening mechanism is due to collisions between molecules (or atoms) in the gas. As the rate and "impact" of these molecular collisions are highly dependent on the absolute gas pressure, collisional broadening is also referred to as pressure broadening.

A physical explanation for part of this broadening effect is closely related to the natural broadening which, as said, is due to the inherent, limited (mainly upper-state) lifetime. However, the effective lifetime is usually much shorter than that, due, for example, to the frequent collisions that occur between the molecules in a gas at normal pressures. As the lifetime is reduced by these inelastic collisions, it is reasonable that the absorption/emission lines are broadened, simply following the theory in Sect. 3.1.3. The collisional relaxation rate, Γ_{col} describes the probability for collision induced de-excitation from a certain energy level.

Γ_{col} is obtained from the number density, N/V of molecules of the considered species of collision partner,[2] the collision cross-section, σ_{col} and the average, relative velocity,[3] $\langle v \rangle$, according to

$$\Gamma_{col} = \frac{N}{V}\sigma_{col}\langle v \rangle. \tag{3.18}$$

Using

$$\langle v \rangle = \sqrt{\frac{8k_B T}{\pi \mu}}, \quad P = \frac{N}{V}k_B T, \tag{3.19}$$

where μ is the reduced mass of the collision pair, and P is the partial pressure of the collision partner species. We obtain

$$\Gamma_{col} = \frac{N}{V}\sigma\sqrt{\frac{8k_B T}{\pi \mu}} = P\sigma\sqrt{\frac{8}{\pi \mu k_B T}}. \tag{3.20}$$

Thus (see, e.g., Eq. (3.6)), the width is linearly increasing with pressure (T constant) in the regime where pressure broadening is dominant (approximately above 0.1 atm in the IR-region). Further, since the autocorrelation function has the same expression, the lineshape for a pressure broadened line is also Lorentzian.

Although the above explanation is reasonable, it does not account for the full phenomenon (as has long been known; see e.g. Ref. [39]), and the deviation from this theory is actually used in some of the work in this thesis.

Measurements have shown that pressure broadened lines are not always well represented by symmetric lineshapes, and that not only the width of an absorption line is altered, but also the peak position – we have a line *shift* too. Furthermore, a careful study shows that the collisional broadening and shift of an absorption line belonging to a molecule depend not only on the total pressure, but also on who its neighbor molecules are. In other words, the collisional broadening and shift are dependent on the gas *composition*.

To explain these observations, the interaction potential between the colliding molecules must be considered. When two

[2] If more than one species is considered, which should be the case as long as one collision partner is not very dominant, a sum of the contributions must be made.

[3] Inserting the average relative velocity in this equation leads to an approximation where it is assumed that every collision completely interrupts the radiation [35, 38]. This approximation is also a prerequisite for claiming that collisional broadening is homogenous, since the individual speeds of each molecule would otherwise affect their de-excitation probabilities.

molecules are in the vicinity of each other, forces will arise, similar to the force between the atoms in Fig. 3.2. The different nature of these forces can in special cases lead to covalent bonds or hydrogen bonds, if the interacting molecules allow for that. When ions are involved, electrostatic forces arise. When none of these forces are present, the "rest" of the attractive or repulsive forces are (often) referred to as *van der Waals forces.* The van der Waals forces are traditionally said to be created between electronically neutral molecules which act as dipoles (permanent or instantaneous). The force can arise due to the interaction between two permanent dipoles[4] (e.g., between two water molecules), between one permanent dipole and one induced dipole[5] (e.g., one water and one oxygen molecule), or between two induced dipoles[6] (e.g., two oxygen molecules). The two latter cases will always give an attractive force. At normal temperatures these attractive forces are too weak to bind the atmospheric molecules to each other; however, they constitute the reason why gases turn into liquids at low enough temperatures.

[4] Keesom force

[5] Debye force

[6] London force

These forces will shift the molecular energy levels – if the force is attractive, the energy will be lowered (for both involved molecules), and if repulsive, the energy raised. The magnitude of the potential energy due to the molecular interaction depends on the polarizability (which is anisotropic and frequency-dependent) and the multipole moments[7] of the molecules. Two permanent dipoles interact strongly, leading to a large broadening when the concentration of such molecules is high. On the other hand, in the case of O_2, which has no permanent dipole moment, the quadrupole moment is instead the leading multipole term, generally leading to a weaker broadening [35].

[7] The expansion of the charge distribution of the molecule into the net charge, dipole moment, quadrupole moment, octupole moment, etc.

As the energy shift in this type of interaction is specific for each level, the transition frequency is also shifted. The result is that collisions can induce frequency shifts, in addition to the broadening discussed above.

The use of autocorrelation functions enables implementation of shifts in the calculation of the lineshape by adding an imaginary part, Λ, to the autocorrelation function:

$$\Phi(t) = \exp(-(\Gamma + 2\pi i(\Lambda - \nu_0))t). \qquad (3.21)$$

The effect of such an implementation is seen in Fig. 3.6 where $\Delta\nu$ and $\delta\nu$ indicate the FWHM and line shift, respectively.

The complex relaxation matrix, $\Gamma + i\Lambda$, is correctly obtained by performing an average of all the collision parameters according to

$$\Gamma + i\Lambda = \frac{N}{V}\left(\langle v\sigma'\rangle + i\langle v\sigma''\rangle\right). \qquad (3.22)$$

Here σ' and σ'' are the collision cross sections related to broadening and shift, respectively ($\sigma = \sigma' + i\sigma''$ is the differential col-
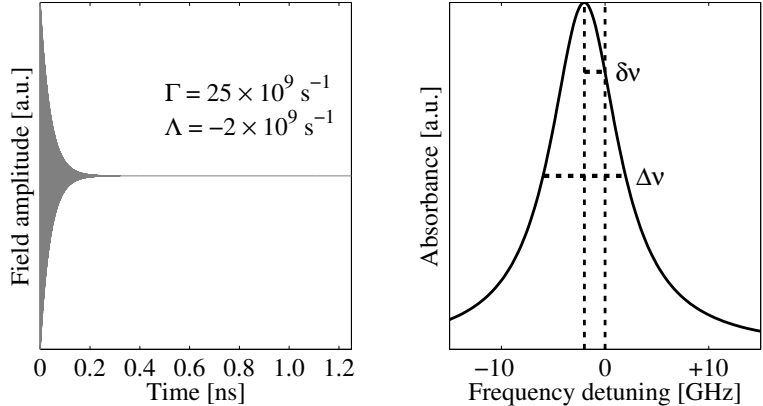
Figure 3.6. *The use of an autocorrelation function with both a real (Γ) and an imaginary (Λ) part in the exponent leads to both broadening and shifting of the line.*

lision cross section), v is the relative velocity of the molecule pair and, again, N/V is the number density of the perturbing molecules. If (as in Eq. (3.20)) the approximation that the cross section is independent of v is made, Eq. (3.23) is obtained.

$$\Gamma + i\Lambda = \frac{N}{V} \langle v \rangle (\sigma' + i\sigma'') \tag{3.23}$$

Where $\langle v \rangle$ is the average thermal relative velocity given by Eq. (3.19). This indicates that also the shift is approximately linear to the partial pressure of the perturbing molecule. This is in good agreement with experimental data (such as in Ref. [40]).

Since these approximately linear dependencies between the line's width and shift and the pressure exist, the pressure broadening coefficient, γ (e.g. [Hz/atm]), and pressure shift coefficient, δ, have been introduced. These coefficients have been given great attention, and are tabulated for various molecule pairs and transitions. Special attention has been given to water vapor since it has such a large influence on radiative transfer in the atmosphere [41, 42].

In the case where a mixture of gases forms the buffer, there will be a statistical contribution to the pressure broadening and shift from the different molecular components. When the gas only contains one molecular species, the broadening and shift are referred to as self-broadening and self-shift, respectively. Another example where the coefficient has been given a special name, is when the measured molecule is surrounded by air, i.e. 78% N_2, 21% O_2 and 1% Ar. The coefficients are then referred to as air-

broadening and air-shift coefficients, respectively. For the latter example, measurements are often performed by actually using air as buffer, although the contribution from each neighbor species can also be measured individually. In that case the total coefficient is approximately given by a weighted sum.

Fig. 3.7 shows an illustration of how the width and center position are changed with pressure. The integrated absorption is kept constant for all pressures, something which is true only if the increased pressure is due to a higher density of other types of molecules than the absorbing one.

Fig. 3.8 shows how the absorption depends on the species of neighboring molecules, at a constant pressure (1 atm). The figure shows peak-normalized laboratory data of a water vapor absorption line at ~935 nm, obtained with the laser spectroscopic technique TDLAS, discussed in Sect. 4.1. The spectra are obtained with ~2% water vapor mixed with ~98% CO_2, N_2 or O_2, respectively. Note that, again, both width and peak position are affected. For thorough investigations of the broadening phenomenon, higher order multipole moments (than the charge and dipole) must also be considered. As an example, N_2 has a larger quadrupole moment than O_2, so the interaction with the dipole H_2O is stronger – this is part of the reason for the broader H_2O line in the N_2 mixture in Fig. 3.8.

Figure 3.7. *Both width and center position are affected by the total pressure of the gas. The curves are normalized to their areas.*

Resulting lineshape

The absorption line of a gas molecule is, of course, affected by all of the phenomena described so far at the same time. This results in a lineshape consisting partly of a Lorentzian shape due to the natural broadening, but mainly due to the shortening of the effective lifetime and shifts during collisions with other molecules; and partly consisting of a Gaussian shape arising from Doppler shifts of the moving molecules. As mentioned, the pressure broadening is often dominating at ambient pressures. As an example, the lines in the oxygen A-band (which are much used in this thesis work) have the approximate values $\Delta\nu_D \sim 0.5$ GHz and $\Delta\nu_P \sim 3$ GHz (FWHM) at ambient conditions [43, 44]. No analytical expression exists that can describe the resulting lineshape where both these effects are considered. The resulting profile is therefore often obtained through a convolution between $\chi_P(\nu)$ and $\chi_D(\nu)$, i.e.,

$$\chi_V(\nu) = \chi_P(\nu) * \chi_D(\nu) = \int_{-\infty}^{\infty} \chi_L(\nu')\chi_G(\nu - \nu')d\nu'. \quad (3.24)$$

This results in the Voigt profile; see Fig. 3.9. When using the autocorrelation approach, Φ_P and Φ_D can simply be multiplied, resulting in

Figure 3.9. *The Voigt profile is the result of a convolution of a Gaussian and a Lorentzian profile. Voigt_same is a Voigt profile with the same width (at $1/e$) as the Gaussian and Lorentzian curves, while Voigt_res is the actual result of the convolution between the Gaussian and Lorentzian curves shown here. All curves are normalized to their areas.*
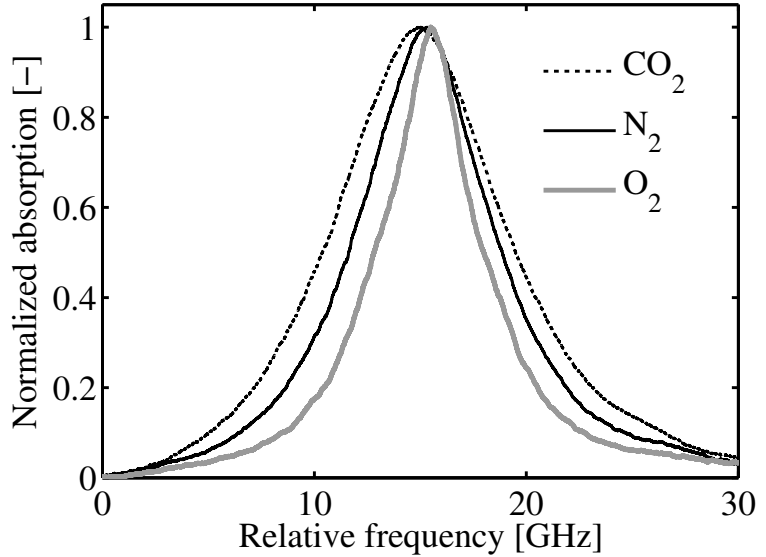
Figure 3.8. *Laboratory measurements of the absorption line shape of a water vapor line at 935 nm for different neighbor molecules, but at the same total pressure (1 atm). The curves are normalized to their peak values. The data are unpublished but were obtained in connection to the study presented in* **IX***.*

$$\Phi_{\mathrm{V}}(t) = \exp\left(-(\Gamma + 2\pi i(\Lambda - \nu_0))t - \left(\frac{v_{\mathrm{A}}t}{2\lambda}\right)^2\right) \qquad (3.25)$$

When fitting the Voigt profile to experimental line shapes, it is common to fix the Doppler width to its theoretical value (Eq. (3.16)), and only allow the pressure related parameters to be adjusted. Although the Voigt profile usually can reproduce most lineshapes with very little error with $\Delta\nu_{\mathrm{D}}$ fixed, high resolution spectroscopic studies, both in the microwave [45, 46] and IR regions [47, 48] have revealed deviations from this theory. A reason for the discrepancy is the so-called Dicke narrowing [49], where the Gaussian part is reduced at higher pressures because frequent collisions decrease the average molecular speed in the gas.

Using the autocorrelation representation, Dicke narrowing can be implemented by inserting a pressure-dependent weighting function for the Doppler term in the exponent of Eq. (3.25). This function depends, for example, on the relative masses between the colliding molecules. In the "soft collision"/Galatry regime [50] it is assumed that many collisions are needed to significantly reduce

the speed of the absorber molecule (which in practice means that the absorber is heavier than its collision partners). In the "hard collision" regime [51] it is instead assumed that the collision is so significant that the initial velocity is completely lost and the speed is returned to that given by Eq. (3.12). Other detailed models also exist which, e.g., include the fact that the collision cross section can be speed dependent, i.e., Eq. (3.23) is not used. This improvement can be performed in combination with the Voigt (speed-dependent Voigt, SDV) or the Dicke-compensated profiles (Speed-dependent Galatry (SDG) and speed-dependent Rautian-Sobelman (SDR), for the soft collision and hard collision regimes, respectively). The speed dependency of the collision cross section can lead to asymmetric lineshapes.

Actually, for the oxygen lines around 760 nm (used in this work), there can be a difference in resulting width of up to 2.5% when fitting the Voigt and Galatry profiles (buffered in $P = 0.6$ atm of pure oxygen at room temperature; smaller difference at higher pressure) [43].

3.2   Fluorescence

Fluorescence occurs whenever a substance that has absorbed a photon emits this energy as another photon. The most commonly observed type of fluorescence is when the emitted light has a longer wavelength than the absorbed, i.e. the emitted light is Stokes-shifted.[8]   This phenomenon occurs frequently in our daily lives since almost all natural (e.g. biological) substances are more or less fluorescent. Fig. 3.10 shows the principle of Stokes-shifted fluorescence. A photon with high energy excites the substance (atom or molecule) to a higher electronic level or band of levels. Frequently, a very fast series of non-radiative transfer mechanisms leave the substance in the lowest level of the excited electronic band before the fluorescence light is emitted. The fluorescence can be composed of one or many sharp lines (as the upper part of the figure would suggest), but in the case of solid materials, the possible energy levels are smeared into a continuum of levels, which means that any wavelength in a certain interval could be emitted. When a large set of molecules are excited with a large number of photons, the total emitted fluorescence is thus composed of a broad, continuous distribution of wavelengths, as is seen in the bottom part of Fig. 3.10.

In addition to Stokes-shifted emission, *resonant* fluorescence can also occur, where the emitted photon has the same wavelength as the one absorbed. A less common phenomenon is when multiple (usually two) photons are simultaneously or stepwise absorbed so that a photon with higher energy may be emitted, i.e. an anti-Stokes-shifted emission.[9] These latter types are, however, not encountered in this thesis and are not further discussed here.

The light emitted following excitation by a particular wavelength contains much information about the fluorescing substance. Fluorescence can thus be used for molecular identification, and is indeed a much exploited and powerful tool for this purpose. The most commonly used properties of the fluorescence for molecular identification are the spectral shape and the decay time of the emission, following excitation by a short laser pulse.

In the work of this thesis, the spectral shape (the spectrum) of the emitted light following excitation by UV laser radiation is used for species identification and classification of solid materials (Papers **XIII**, **XIV**, **XV** and **XII**). The spectrum of light actually emitted by an object depends both on the spectrum of the primary fluorescence by the fluorescing molecule, and on the spectrum of possible re-absorption by the fluorophore, and other molecules in the object. These two types of phenomena (which in reality often occur in combination) are illustrated in Fig. 3.11. In practice, it is often very difficult to distinguish between the phenomena.

[8] Sir George Gabriel Stokes, observed visible light emission by fluorite after UV-light excitation in 1852 and gave the phenomenon the name fluorescence [52].

[9] Examples are stepwise excitation for studies of alkali-metals [53], upconverting nanoparticles, e.g., [54–57].
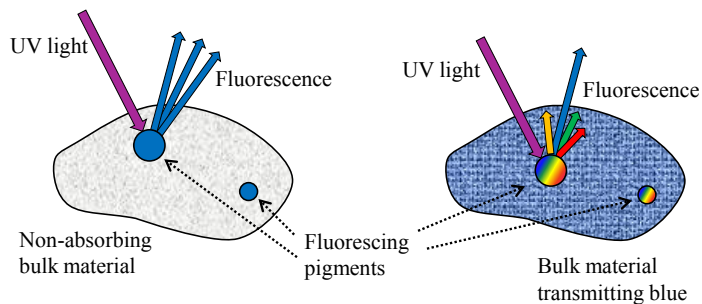
Figure 3.11. *A colored fluorescence from an object can arise in two ways, as in the left and right parts of the figure. In the left part, the bulk has little absorption but the fluorescence is restricted to the blue part of the spectrum. In the right case, the initial fluorescence by the fluorophore contains many colors but the bulk absorbs all but blue.*
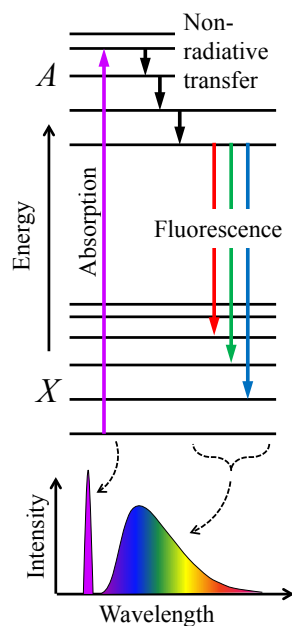
Figure 3.10. *The principle of fluorescence. The upper part shows an energy level diagram. The (often) ultraviolet excitation photon excites the molecule. Once in the excited state different paths for de-excitation can be taken. The many possible energies for emitted photons generate a multitude of emitted wavelengths. In solid or liquid matter the infinite amount of possible energies induce a continuous emission spectrum, as seen in the bottom part of the figure. (Note, the quantized nature of the energy level diagram does not agree fully with the bottom part.)*

Basic techniques for optical spectroscopy

The aim of this chapter is to describe the principles of the most important "basic techniques" on which our methods are based. By basic techniques is meant the well-established spectroscopic techniques that form the foundation to the specialized systems and techniques used in the thesis work.

4.1 Tunable diode laser absorption spectroscopy

When probing gases using a light source where a broad range of wavelengths are emitted simultaneously, a detection system which distinguishes between wavelengths must be used. Another approach would be to use a light source where the emitted wavelength is changed as function of time. Tagging the detected intensity in time, will then enable a spectroscopic measurement without sorting any wavelengths with the detector. This approach inherently enables the use of large area detectors, which is of great importance to the GASMAS technique (Chap. 5). The introduction of tunable lasers in general has, in principle, made this approach the obvious choice in most situations where a fast and sensitive gas measurement should be made at high wavelength resolution. Tunable diode lasers are, since their first development in the 1960's, often particularly suitable for the task. This section will introduce the principle and general theory of tunable diode laser absorption spectroscopy (TDLAS).

A review of industrial applications of TDLAS may be found in Ref. [58], a general description in Ref. [59] and an overview of approaches for sensitive detection in Ref. [60]. The equipment used for TDLAS (lasers, detectors, amplifiers, etc.) is certainly

Figure 4.1. *The fundamental principle of TDLAS.*

1

http://www.cfa.harvard.edu/hitran/

[2] The absorbance is originally defined as the decadic logarithm of the ratio between the intensities in the absence and presence of absorbers, i.e., $A \equiv \log_{10}(I_0/I)$, and the exponent in Eq. (4.1) should therefore be multiplied by $\log_{10}(e)$ to become the original absorbance.

[3] This is generally true at low optical depths with low absorbance, but needs closer investigation for high optical depths, especially when using modulation techniques [66], as will be discussed later.

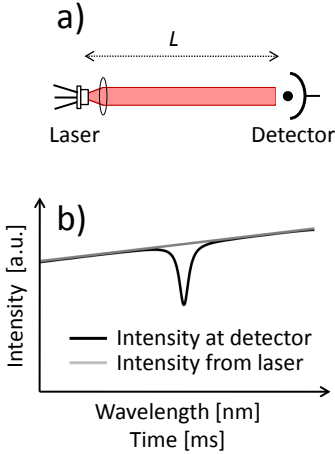of great importance, and have to be chosen with care. However, the physics, construction and performance of these components will not be elaborated on in this thesis as these aspects are well covered, e.g., by many previous theses from our group; see, e.g., [44, 61–64].

4.1.1 Fundamental principles of TDLAS

The general implementation of TDLAS is to tune the wavelength of the laser across a wavelength interval where the probed gas has an absorption line and the light is sent along a path through the gas. A detector records the intensity of the light that passed through the gas as a function of time. At the time of the scan when the laser wavelength matches the gas absorption line, a lower intensity is recorded; see Fig. 4.1. The fraction of light lost at the absorption line, is dependent on the concentration, c, of the gas and the path length of the light through the gas, L. This relationship is given by the Beer-Lambert law [65].

$$I(\lambda) = I_0(\lambda) \cdot e^{-\sigma(\lambda) \cdot c \cdot L} \tag{4.1}$$

This equation can be written in many ways, depending on the choice of units, but if the path length is given in centimeters, and the concentration in molecules per cm^3, σ must have the unit cm^2 for the exponent to be dimensionless. This would then be the absorption cross section of the molecule as function of wavelength. σ is an inherent property of the molecule, and much work has been devoted to measuring and/or calculating its value for different conditions (such as temperature or pressure). To collect and merge the results by different scientists, a large, open-source database with the name HITRAN (high-resolution transmission molecular absorption database) has been created where the absorption cross sections for numerous molecules and transitions may be found[1].

When performing a TDLAS measurement, the most common property of interest is the gas concentration. To extract the concentration from the measured intensity decrease, both ϵ and L must obviously be known. In most cases, when the laser beam passes in a straight line along a well defined path, L is physically measured. ϵ could, in principle, be known from databases such as HITRAN, and indeed sometimes this is the way to proceed. However, it is probably more common to perform calibration measurements with known gas concentrations. The main advantages of this approach is that it is then not necessary to know exactly which absorption line of the gas is being monitored, and that the whole signal processing chain is automatically considered in the calibration [67]. Since the absorbance[2] $(= \sigma(\lambda) \cdot c \cdot L$, using the above version of the Beer-Lambert law) is directly proportional to concentration, and the final TDLAS measurement result is approx-

imately linear to the absorbance, a single or double point reference is often enough.[3]

The simple method described above, where the laser is tuned in wavelength and the intensity directly measured, is seldom used when the absorption is weak, i.e. when $I(\lambda) \approx I_0(\lambda)$ (which is a normal case for TDLAS). The main reason is that a very small reduction of a comparatively large detected intensity must be detected, a method which is inherently sensitive to noise. It would be better if one could measure a signal rising from a zero background.

A common way to achieve a low-background measurement is by using modulation techniques, such as the very well established method wavelength modulation spectroscopy (WMS) [68]. The WMS technique has several advantages over the simple implementation of TDLAS presented above.

A new approach to achieve a zero background measurement with TDLAS, which uses an interferometer, is presented in Paper **I**.[4]

4.1.2 Wavelength modulation spectroscopy

The essence of WMS is to rapidly modulate the wavelength of the laser in a sinusoidal manner, at a frequency f_m. As the transmittance is highly wavelength dependent when close to the resonance of an absorption line, the transmitted intensity will thus also "fluctuate" when the laser is close to resonance. The modulation in the detected intensity can be found with a lock-in amplifier. Due to residual amplitude modulation (RAM)[5] which is inevitable for most diode lasers, the intensity will vary sinusoidally at f_m even without absorbing molecules. However, the amplitude of the modulation at f_m will be changed around the absorption line. Due to the strong non-linearity of the molecular absorption feature, the transmitted intensity will also contain higher order modulation components [69]. Since RAM is often close to linear, these higher order components are in fact close to zero in the absence of absorbers, or when the laser wavelength is far from the absorption line. Employing WMS and scrutinizing the signal for intensity modulations at $n \times f_\mathrm{m}$, where $n = 2, 3, ...$, thus provides a quasi zero background approach to the TDLAS technique.

As mentioned, to measure the degree of modulation at the overtones of f_m, the detector signal is traditionally sent to a lock-in amplifier. Another major advantage of WMS is thereby clear. The lock-in amplifier is only sensitive to modulations around the chosen frequency (e.g. $2 \times f_\mathrm{m}$) and thus, ideally, noise with frequencies above and especially below this frequency will be ignored. Employing a reasonably high modulation frequency (e.g. some ten kHz), will thus move the detection to a region where the $1/f$ noise of the laser is drastically decreased. If f_m is chosen so high that it becomes comparable or even larger than the width of the absorp-

[4] The technique is based on dividing a laser beam into two arms with exactly the same intensities, of which one beam passes through a gas sample and the other through a reference path of the same length. The two beams are combined again to create an interferometer (Michelson or Mach-Zehnder). In case of no absorption the beams cancel the detected intensity completely through destructive interference. In case of gas absorption, the two intensities are no longer matched and the detector receives a small light signal.

[5] Since the wavelength is generally tuned by changing the injection current through the diode, the intensity of the light is increased for longer wavelengths.
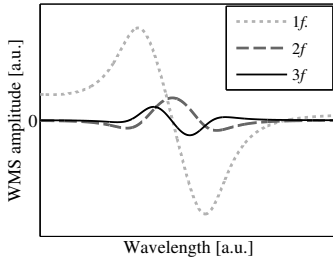
Figure 4.2. *WMS example curves for the three first components ($1f, 2f$ and $3f$), generated through a simulation with $m = 2.2$ for a water vapor line at 819.15 nm.*

tion line (up to some GHz), the signal generation process starts to differ from that at lower modulation frequencies. In this regime the technique has therefore been given another name – frequency modulation spectroscopy (FMS) [70]. Although the theoretical sensitivity of FMS is better than that of WMS, technical practicalities due to the high frequencies involved in FMS, are often working in favor for WMS [71–73]. FMS is not used in the work of this thesis.

The common way to employ WMS in TDLAS is to use an injection current consisting of a sum of a slow linear sweep, with frequency f_{scan}, and the fast sinusoidal modulation. The output voltage of the lock-in amplifier is then recorded as a function of the sweep-time, creating a wavelength dependent lock-in signal. If the modulation amplitude is small compared to the width of the absorption line, i.e. using a small modulation index[6], m, the output of the lock-in amplifier is proportional to the n:th derivative of the absorption feature. In this limit, where $m \ll 1$, the modulation method is therefore referred to as derivative spectroscopy [74]. In practice, however, the modulation index is generally raised to increase the amplitude of the lock-in signal and improve the signal-to-noise ratio. For Lorentzian, Gaussian and Voigt line shapes, it has been shown that the maximum $2f$-WMS amplitude (i.e. the lock-in amplitude at $2 \times f_{\text{m}}$) is obtained with $m = 2.2$ [74]. The WMS curves will still resemble the derivatives when using larger m, but only approximately.

Fig. 4.2 shows an example with the typical appearance of the three first WMS curves, $1f, 2f$ and $3f$.

In recent years it has become common not to use analogue lock-in amplifiers but to instead sample the raw signal from the detector and perform the lock-in procedure in a digital manner afterward. The technique is then commonly referred to as digital wavelength modulation spectroscopy, dWMS. If more than one sweep are averaged before analysis, it is crucial that the modulation phase with respect to the sweep is the same in all sweeps.[7] Instead of averaging the lock-in signal from many sweeps, the raw signals from those sweeps are averaged and sent to digital analysis. An advantage of sampling the entire signal is that the lock-in can be performed on more than one harmonic without using multiple analog lock-in amplifiers. It is common to perform major parts of the digital analysis by means of Fourier analysis, but it is also possible to do an efficient analysis without this. Very short descriptions of two possible ways to proceed by are given in the following subsections.

_____

[6] $m = \nu_{\text{a}}/\Delta\nu$, where ν_{a} is the amplitude of the modulation and $\Delta\nu$ is the HWHM of the absorption line.

[7] This is guaranteed through so called coherent sampling [75, 76].

dWMS analysis by means of sine wave multiplication

The basic function of an analog lock-in amplifier is to instantaneously multiply the measured signal with a perfect reference sine

wave. The frequency of the reference wave is set to the lock-in frequency, $n \times f_m$. The phase of the reference wave is set to maximize the WMS signal amplitude. The result of this multiplication is then sent through a low-pass filter, so that the integrated result over a certain time interval composes the output signal.

The same approach can, of course, be used in digital analysis. In this case, a perfect sinusoidal (or square) wave with frequency $n \times f_m$ is created and centered around zero. This wave is multiplied with the sampled signal and the result is integrated over a certain number of sampling points. The time-window of this integration will affect the bandwidth of frequencies which are accepted. The phase of the reference sinusoid must be adjusted for optimal signal generation. A drawback with this approach is that it is more difficult to perform this phase optimization, than with the Fourier approach. The analysis could be implemented to perform close to real-time analysis to present the dWMS result on the screen while recording a measurement, similarly to when using analog lock-in amplifiers. The method is then enabled through a digital phase locked loop (dPLL), which could, e.g., be implemented using LabView [76, 77].

Fig. 4.3 shows the principle of the sine wave multiplication approach, using laboratory data from an oxygen measurement. A modulation frequency of 10,295 kHz and a sampling frequency of 400 kHz were used. Included in the figure is a small time section of the signal from the detector where the DC component has been subtracted to place it around zero. The included section is collected from the peak of the absorption line. A reference sine wave with frequency $2 \times f_m$ is multiplied with the detector signal and the result is a curve ("Mult. max") essentially varying around zero. However, integrating this curve across this region results in a small positive value, reflecting the peak value of the WMS curve (i.e. a very short region around the peak of Fig. 4.2). Included in the figure is also a corresponding multiplication curve, but this time collected from a region outside of the absorption line ("Mult. zero"). This curve is similar to the other but slightly lower at places, leading to an integration which is exactly zero.

dWMS analysis by means of Fourier methods

The Fourier approach for dWMS analysis was implemented as a means to deal with rapidly changing transmissions in WMS [75]. The method is extensively described in the literature and in other theses from our division where WMS has been used; see, for example Ref. [78], and will therefore be only very briefly introduced here, following the approach of Ref. [79]. Let $u(t)$ denote the sampled voltage signal as a function of time; see Fig. 4.4a. The digital Fourier transform of $u(t)$, $U(\omega)$, is complex and thereby contains the amplitude and phase of all the frequency components.
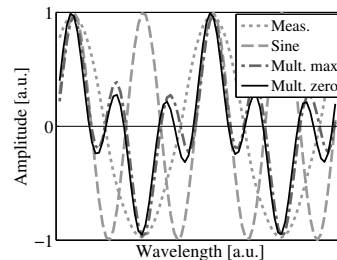
Figure 4.3. *The measured signal ("Meas.") has the overall appearance of a sine wave with frequency f_m (due to the RAM). The curve "Mult. zero" is obtained by multiplying a section of the measured signal outside of the absorption line with a perfect sinusoid ("Sine") with frequency $2 \times f_m$. "Mult. max" is obtained through the same principle but instead using a section of the measured signal on the peak of the absorption line. The two multiplication curves are slightly different and an integration leads to a slightly positive result for "Mult. max", and exactly zero for "Mult. zero". These values, extracted for the whole signal, make up the 2f WMS curve.*
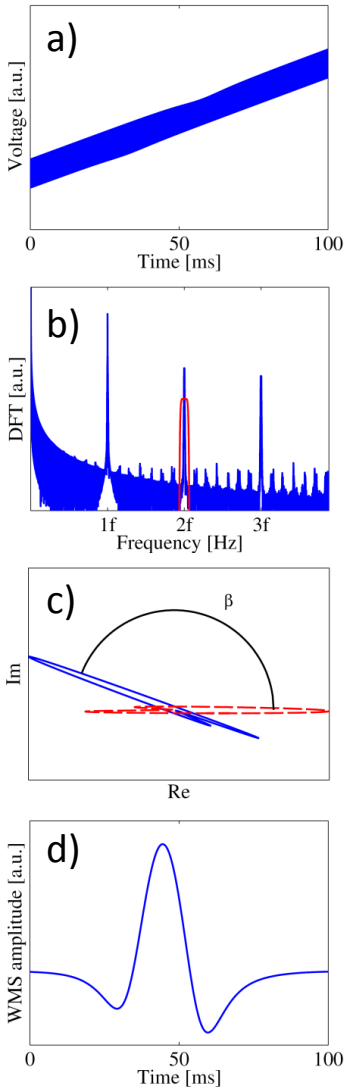
Figure 4.4. *The principal steps of one way to perform Fourier-based WMS demodulation. a) shows the raw detector signal (after the amplifier), b) is the digital Fourier transform of the detector signal, c) represents the "phase-amplitude" plot given by Eq. (4.4), and d) is the final, demodulated WMS curve.*

$$U(\omega) = \mathfrak{F}\{u(t)\} \qquad (4.2)$$

The absolute value of $U(\omega)$ is shown in Fig. 4.4b, together with a band pass filter function at $2f$, which is used to select the desired harmonic component. $U(\omega)$ is multiplied with this band-pass filter, which could be as a super-Gaussian function according to

$$U_{nf}(\omega) = 2 \times U(\omega) \times \exp\left(-\left(\frac{\omega - 2\pi n \times f_{\mathrm{m}}}{\delta\omega}\right)^8\right). \qquad (4.3)$$

Here, $\delta\omega$ is the width of the band-pass window. To obtain the degree of modulation at frequency f_{m} as a function of time (wavelength) in the sweep, the content of $U_{nf}(\omega)$ at f_{m} is shifted to zero frequency, and the inverse Fourier transform is obtained.

$$v_{nf}(\omega) = \mathfrak{F}^{-1}\{U_{nf}(\omega + 2\pi n \times f_{\mathrm{m}})\} \qquad (4.4)$$

v_{nf} is complex and contains both the phase and amplitude of the evolution of the harmonic component. The imaginary part of the $2f$ component is plotted versus the real component in Fig. 4.4c. To obtain the final WMS curve, v_{nf} is turned in the complex plane to align with the real axis, by multiplication with $\exp^{-i\beta}$. One of the advatages with the Fourier approach is that in many cases it is quite simple to find β. The amplitude along the real axis as a function of time (wavelength) gives the usual $2f$ WMS curve, seen in Fig. 4.4d.

In Fig. 4.5 a WMS recording of an oxygen line at 760 nm has been analyzed with these three different approaches. The voltage from the detector unit was split into one part that went to an analog lock-in amplifier, while another was sampled directly. The latter was analyzed with both the sine wave multiplication and the Fourier approach, showing good agreement.

4.2 Frequency modulated continuous wave ranging

This section briefly introduces the background to a technique which was developed and used in Papers **VI**, **VII** and **VIII**, to measure optical paths in light scattering materials. The need for this information and the motivation for the choice will become clear in Chap. 5.

Heterodyne techniques refer to methods where two waves of any kind are mixed together so that sum and difference frequency waves are generated. The method originates from the radio field, and was invented by Fessenden and colleagues for down-converting continuous wave (CW) radio frequency signals to frequencies that
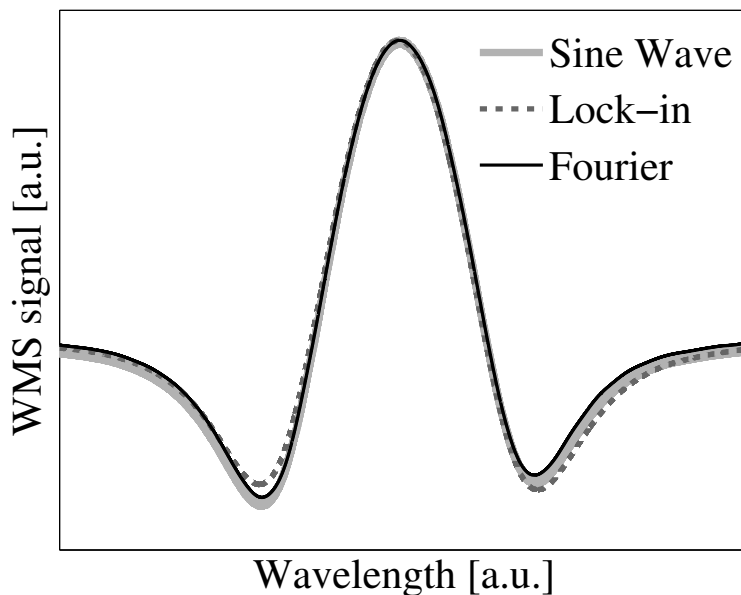
Figure 4.5. *Examples for three ways to extract a $2f-WMS$ curve: (i) Using an analog lock-in amplifier ("Lock-in"), (ii) multiplication with a sinusoidal wave with frequency $2 \times f_m$ ("Sine Wave"), and by Fourier transform methods ("Fourier"). The exact shape of each curve depends, e.g., on the integration time in the lock-in and the width of the Fourier window function.*

could be listened to [80]. A local oscillator (Beat frequency oscillator, BFO) in the radio device is mixed with the incoming radio wave.

As two waves with frequencies f_1 and f_2 interfere, among others, a resulting amplitude fluctuation at the difference frequency, $|f_1 - f_2|$, can be observed. This phenomenon may be referred to as "beating" – the acoustic origin of the term is apparent.

Several methods use the heterodyning phenomenon to measure distances, including the CW versions of sonar [81] and radar [82, 83]. The simplest radar version is here taken as an example. In the frequency-modulated CW radar, the frequency of a radio wave is rapidly tuned with, for example, a sawtooth chirp. A part of this wave is transmitted and reflected from a target. The received wave is mixed with another part which was split off. Since the transmitted wave has traveled further, its mixing component originates from a part of the sawtooth chirp which was sent out earlier, and thus has a lower frequency. The difference in frequency is given by

$$f_{\text{b}} = 2nRf_{\text{scan}}\Delta\nu/c_0. \tag{4.5}$$

Here, n is the refractive index, f_{scan} is the scanning frequency, $\Delta\nu$ is the range of optical frequencies scanned and c_0 is the speed of the electromagnetic wave in vacuum. The distance, R, can thus be obtained from the beat frequency.

The principle above would, of course, be applicable also for optics, since only the frequency differ a radio wave from light. However, a tunable, narrow-band light source is required. With the introduction of tunable near-infrared diode lasers, the technique was transfered to the fiber-optical community. Here it has been used for reflectometry [84], for example to search for poor fiber joints.

4.3 Light detection and ranging

The principle of the technique LIDAR [85, 86] is similar to that of radar. Instead of the radio waves used by radars, a LIDAR system typically emits short laser pulses which are reflected from, or scattered from, some kind of target. A telescope which is positioned close to the laser, or even co-axially with the laser beam, focuses the reflected or back-scattered light onto a detector (typically a PMT) that gives the intensity as a function of time, t. The fundamental principle of a general LIDAR is shown in Fig. 4.6, where the target in a) is a solid wall, giving a sharp intensity peak at a certain time, given by $t = 2R/c$, with R being the distance to the target and c the light speed. In this mode, with a solid target and detection of the same wavelength as that emitted (i.e. elastic LIDAR), the technique can be used for "trivial" ranging, e.g. for military purposes, 3D-mapping of buildings, grottoes, vegetation, etc. Also seen in the detected signal is the back-scattering from atmospheric molecules, which has a $1/R^2$ dependence[8]. This signal is, of course, basically zero after the wall echo.

In Fig. 4.6b the target is no longer solid, but is a distributed cloud of, e.g., aerosols, or single molecules. Light scattering in the cloud will spread photons in all directions[9]– a fraction of the photons will be scattered toward the telescope and detector, which in this case will show a broad time distribution of the signal. As the detected light intensity might now be very low, it is important to use a sufficiently large telescope and a sensitive detection. This type of elastic back-scattering LIDAR is typically used for atmospheric research where the scattering coefficients at different laser wavelengths[10] can provide information about the size and altitude distribution of atmospheric particles.

Actually a technique combining FMCW and LIDAR, exist [87], mainly for discrete targets, but has been proposed even for distributed targets [88].

[8] The shape of the back-scattering curve by a homogenous atmosphere is dependent on system parameters. The number of photons reaching the telescope is indeed decaying as $1/R^2$. However, the throughput is generally lower for shorter distances, because focus is set for long-distances – so called "geometrical compression". The signal thus often drops towards zero for very short distances (not seen in the Fig. 4.6, while the effect is included in Fig. 4.7).

[9] The amount of scattering into different solid angles is described by Mie- or Rayleigh theory.

[10] Such as the harmonics of the Nd:YAG laser at 1064, 532 and 355 nm.
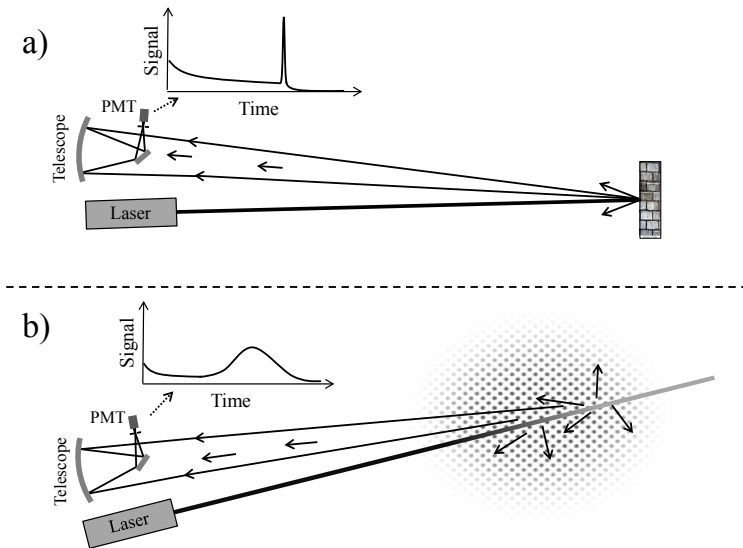
Figure 4.6. *The basic principle of LIDAR measurements. a) shows the echo from a solid wall, and b) shows the echo from a distributed target, such as aerosols.*

Another type of LIDAR, which also is elastic, but somewhat more advanced, is differential absorption LIDAR (DIAL), used for species specific gas absorption detection [89]. The technique was employed for detection of atomic mercury, glyoxal, nitric oxide and nitrogen dioxide in Papers **II** and **III**. Here, the basic idea is to measure molecular or atomic absorptions at different wavelengths, in a similar way as for TDLAS, discussed in Sect. 4.1. However, the pulsed nature of the general LIDAR approach does not allow for sweeping over a whole absorption spectrum, instead only two (or a few) wavelengths are used – "on" resonance and "off" resonance. Alternating pulses of "on" resonance light, having exactly the wavelength of the peak of an absorption line, and "off" resonance light, sitting just outside of the absorption line, are emitted.[11] The extremely small wavelength difference assures that scattering by aerosols, and similar effects, are the same at both wavelengths.[12] Any difference in the R-dependency of the detected light at the two wavelengths should be due to light absorption by the molecule of interest. The number density, N/V, of this molecule is therefore obtained as function of R by the range-derivative of the ratio between the signals $S_{\lambda_{\text{on}}}$ and $S_{\lambda_{\text{off}}}$:

$$\frac{N}{V}(R) \propto -\frac{\mathrm{d}}{\mathrm{d}R}\frac{S_{\lambda_{\text{on}}}(R)}{S_{\lambda_{\text{off}}}(R)} \tag{4.6}$$

[11] A greater number of wavelengths can, in some cases, be employed [90], as was done in Papers **II** and **III**.

[12] Compare to the assumption used in the introduction of the GASMAS technique, Sect. 5.

DIAL was used to measure Hg and NO in Paper **II** and with the aim of detecting $C_2H_2O_2$ in Paper **III**.

Detection of other wavelengths than that of the laser (i.e. in-elastic), enables another set of LIDAR varieties: Wind speed and direction can be monitored by measuring the Doppler shifts of moving particles. The laser-induced breakdown spectroscopy (LIBS) LIDAR utilizes the effect that breakdown can be induced in a material by focusing an intense laser onto a small spot. This induces a plasma that contains ablated material and thereby excited free atoms and ions which emit species specific spectra. Furthermore, the Raman effect can be utilized to observe only the light that is (Raman-) back-scattered by a certain molecule. As an example, the N_2 Raman signal is often used for calibration of the geometrical compression of a certain LIDAR system, since the N_2 concentration is essentially proportional to atmospheric pressure, and thus is known.

An additional LIDAR technique uses the fluorescence phenomenon discussed in Sect. 3.2 – this is laser-induced fluorescence (LIF) LIDAR [91]. Resonant radiation by alkali-atoms in the upper atmosphere has been much studied [92, 93]. Stokes-shifted fluorescence, on the other hand, was used for remote classification of insects and birds in Papers **XIV**, **XIII** and **XV**, and is discussed in somewhat more detail below.

4.3.1 Laser-induced fluorescence LIDAR

LIF-LIDAR generally uses a ns-pulsed UV laser to generate fluorescence in objects to be identified, classified, or in other ways examined. Once excited by the UV pulse, the objects emit their characteristic fluorescence spectra in all directions. Adding a spectrally resolving detection system to the LIDAR telescope therefore makes it possible to obtain information regarding both distance/range distribution,[13] and on the chemical composition of the measured object. Applications of broadband LIF-LIDAR include detection of oil spills [94, 95] and algal blooms at sea [96], vegetation classification [97–99], and condition estimation of historical buildings [100–104].

Fig. 4.7 shows a simulated example of the full, range- and spectrally resolved, information that could be gathered if the measured objects in Fig. 4.6 were fluorescing. Fig. 4.7a shows the elastic signal at the wavelength of the UV laser, at 355 nm, which, again, has a distribution from the general atmosphere,[14] but increases heavily at the position of the wall ($\approx$ 80 m). The fluorescence spectrum of the wall with a broad distribution between 500 and 1000 nm is also seen.[15] Fig. 4.7b shows the same spectral distribution but the distribution of, e.g., the aerosol particles, is included. However, all the information included in the figure is generally not collected in a LIF-LIDAR measurement, as this would require the

[13] For exact (especially short distance) range resolution, the lifetime of the fluorescence also needs to be considered, which will introduce a further delay, making it appear as if the sample is further away than in reality.

[14] This time with "geometrical compression" included.

[15] The amplitude of the elastic signal is heavily underestimated compared to the fluorescence. In practice, the elastic signal must always be suppressed with a long-pass filter.
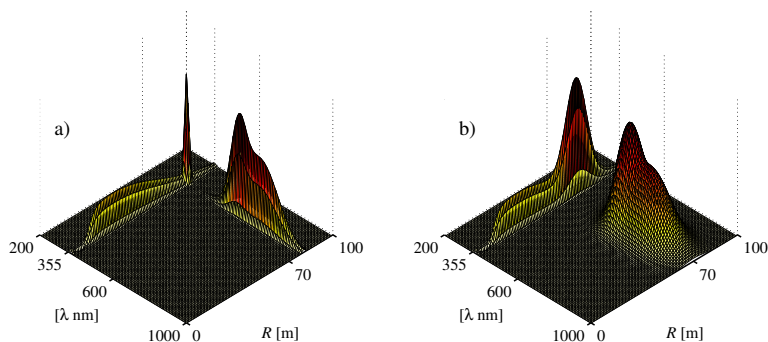
Figure 4.7. *Simulated illustration of the elastic and fluorescence LIDAR returns related to Fig. 4.6.*

Figure 4.8. *The principle of using a system of long-pass filters (band-pass and short-pass are also alternatives) for sorting the light into different spectral channels. Schematic filter transmissions and channel transmissions are included.*

full time-distribution of all spectral channels. In practice, there is always a trade-off between range-resolution, spectral resolution and measurement time (and measurement time resolution).

In cases where the distance to (or the range distribution of) the object is known (e.g., from the elastic LIDAR signal or by other means), the fluorescence spectrum might be the only important parameter. In that case, a fully spectroscopically resolving, sensitive spectrometer can be connected to the telescope output [98, 102]. Time-gating of the signal, or measurement at night, allows for the use of the high gain which is often needed to collect the weak fluorescence signal. In principle, if the target is stationary, sequential shifting of the time-gate window allows for crude range resolution based on the fluorescence. A drawback of the use of diffractive spectrometers is the low sensitivity of the detection unit (typically employing CCDs or CMOS elements).

However, since the fluorescence generally contains quite dull or broad spectral features, it is often not necessary to use all of the channels of the spectrometer (e.g. 1024). Instead a number of rather broad spectral channels that provide as much species specific information as possible can be chosen. The use of a system of dichroic beam-splitters or spectral filters can then separate the different parts of the fluorescence to a number of detectors, as illustrated in Fig. 4.8 (where only long-pass filters are used). Both the spectrometer approach and the use of multiple PMTs were employed for the studies in Papers **XIV**, **XIII** and **XV**. A spectrometer alone was used in Paper **XII**.

Another alternative, which has emerged on the market in recent years are detector systems using PMT arrays (or array multi-anode PMTs). These consist of a linear array of several (e.g., 16 or 32) small PMTs with, say, a diffraction grating separating the
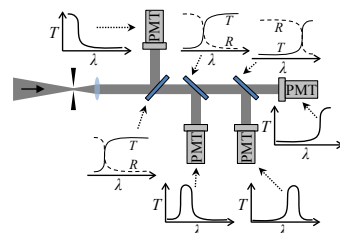
different wavelengths along the array. Except for the light lost in the (mainly) zeroth order diffraction of the grating, the through-put is very high. These systems are often used for the purpose of simply having a very sensitive, time-gateable spectrometer. How-ever, they can also be used for obtaining both range and spectral distribution. Of course, to sample all channels with a rate high enough to allow for good range resolution, places high demands on the sampling electronics.

GAS SENSING IN SCATTERING MEDIA

As discussed in Sect. 4.1, gas spectroscopy is generally performed in well defined geometries, for example with a gas cell, through which a collimated beam of light can be transmitted. Since the path length of the light-gas interaction is then well defined it is possible to apply Eq. (4.1) to find the concentration. There are, however, a great number of cases where a gas of interest is located inside a light scattering (turbid) material. Many objects are porous, meaning that gas (usually air) is enclosed in small pores in a bulk or matrix material. Examples include wood, paper, snow, baking flour, ceramics and medical pills. An equally large number of objects consist of a large gas filled cavity surrounded by a light scattering material, such as a ping-pong ball; a food package made of cartons with a gas head space; a lung, and so on.

In many of these examples it might be of interest to examine the gas content in these pores or larger cavities in a non-intrusive way. X-ray imaging, magnetic resonance imaging (MRI) and, to some extent, ultrasonography (US) are examples of techniques which are excellent in locating gas filled cavities in, say, the human body. However, they cannot provide any information on the gas species. Optical spectroscopy, on the other hand, is very powerful for doing exactly that – providing molecularly specific information. Optical sensing of gases located within light scattering objects is, unfortunately, not very straightforward. At least three problems can be noted – (**i**) it must be possible to pass enough light through the bulk material, (**ii**) it must be possible to distinguish between absorption by the gas molecules and the bulk, and (**iii**) the path length should be known for quantitative concentration measurements, as discussed in Sect. 4.1.1. Although, it might at first seem hopeless to overcome the above problems, the technique GASMAS was introduced in 2001 [105] with the hope that it could be used for laser spectroscopic measurements of gas located in turbid media. Recent reviews of GASMAS are found in Refs [44, 106, 107].
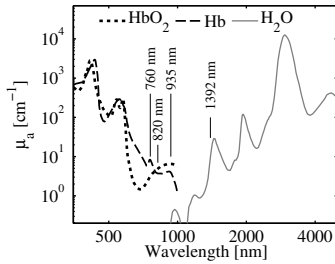
Figure 5.1. *The absorption coefficients for hemoglobin and liquid water. The hemoglobin data have been scaled to give the absorption coefficient of typical whole blood by setting the concentration of Hb and HbO_2 to 150 g/liter blood. Included in the figure are the wavelengths of a few diode lasers used by our group: 760 nm for sensing of O_2, 820 nm, 935 nm and 1392 nm for sensing of H_2O vapor. The strong absorption by liquid water at 1392 nm, however, practically prevents the use of 1392 nm for gas sensing in most biological samples. We can also note that gas sensing of CO_2 at its common bands around 1.6 µm and 2 µm are also practically impossible in wet samples. New possibilities for concentration measurements of, e.g., CO_2, in wet samples are enabled by the approach used in Paper **IX** and discussed in Sect. 5.2.4. Data are collected from Refs [108, 109].*

[1] Except for the Fabry-Pérot type interference fringes which will be discussed later.

It was believed that the three problems above could be overcome in some situations:

i Many materials are reasonably transparent at some optical wavelengths. As an example, much of the GASMAS work has been performed on cavities in the human body. The tissue is actually absorbing the least in a region quite suitable for diode laser spectroscopy. Fig. 5.1 shows data for the absorption of hemoglobin (Hb), oxy-hemoglobin (HbO_2) and liquid water. The region between around 600 and 1400 nm is, thanks to the low absorption of these common constituents, called "the tissue optical window". Furthermore, the ability of techniques like WMS to pick up signals in noisy environments, together with sensitive detectors, and the reasonably high power of today's DFB diode lasers, make it possible to perform measurements even when only one photon out of a million emitted reaches the detector surface. However, in situations where the bulk material does have a reasonably strong absorption, the exponential intensity decrease with path length, makes practical measurements impossible.

ii As exemplified in Fig. 3.1 in Chap. 3, the narrow band nature of gaseous absorption is very different from the broad band absorption features of solid and liquid media. This is one of the key enablers for GASMAS to work.

iii For cases when (**i**) and (**ii**) could be overcome, the inherently unknown optical path length through turbid materials is a difficult problem to solve. The unknown path length of GASMAS measurements is therefore one of the main topics of this chapter.

5.1 Fundamental principle

The greatest difference between "open path TDLAS" and GAS-MAS lies in the measured object, and, as discussed above, this difference induces challenges which need to be addressed. Fig. 5.2 shows a schematic illustration of the principle of gas measurements in turbid media. The left part of the figure shows the straightforward geometry of a gas cell TDLAS measurement. As described in Sect. 4.1, a tunable diode laser is swept across an absorption line of a gas and the intensity is detected as a function of time (and thus wavelength). The windows of the cell have high and spectrally flat[1] transmission so that the detected spectrum clearly reveals the gaseous absorption line.

The middle and right parts of the figure show measurements in turbid media. The injected light is scattered and quickly becomes diffuse, indicated by the diffuse red "halo" around the injection
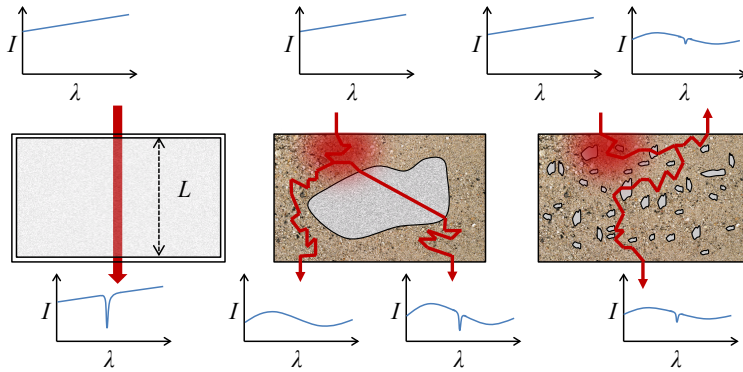
Figure 5.2. *The principle of gas measurements in turbid media. Left: Schematics of a gas-cell TDLAS measurement. Middle: A GASMAS measurement with a single large cavity surrounded by a turbid material. Right: A GASMAS measurement with many small pores surrounded by a turbid material. The slope of the injected light is due to RAM; see Sect. 4.1.*

point. The illustrated trajectories of two individual photons show "random-walk" type paths with frequent direction changes. The bulk material not only scatters the photons but also absorbs light. This is indicated in the figure by the dull, wavy spectral absorption in the detected spectra. The longer the path through the bulk material, the stronger this absorption becomes. The wavelength must be chosen carefully so that the bulk material absorption is as weak as possible, for example taking Fig. 5.1 into consideration. The gaseous absorption is generally much weaker than the bulk absorption, but in many cases the former can still be extracted due to the fundamental difference in spectral width of the absorptions, as discussed in Sect. 3.1.

It is also clear from Fig. 5.2 that the path length in the gas-cell case is simply given by L while for the GASMAS case, it is generally unknown. Furthermore, in the diffuse case, the path length is not the same for all photons, but instead there is a distribution of path lengths. To perform quantitative gas concentration measurements, the average path length of the light-gas interaction must generally be known in one way or another, in order for Eq. (4.1) to be applicable. The following subsections are devoted to different approaches for obtaining the unknown average path length, so that the gas concentration can be calculated from the absorption and Eq. (4.1). A review on this particular subject is found in [110].

5.2 Finding the path length for quantitative measurements

A variety of different approaches have been proposed in order to find the average path length of light-gas interaction, $\langle L_{\mathrm{gas}} \rangle$, in order to facilitate a quantitative concentration measurement using GASMAS. This section will discuss these methods or approaches, here referred to as "Reference calibration on a similar geometry", "Path length calibration with bulk methods" and "Path length calibration with another gas of known concentration". A newly proposed method in which the gas concentration assessment is essentially independent of the path length is also discussed under the subsection "Path length independent measurements".

5.2.1 Reference calibration on a similar geometry

Even if $\langle L_{\mathrm{gas}} \rangle$ is unknown, it can often be considered stable as long as the measurement geometry is kept the same. One very straightforward and, when applicable, simple approach is thus to perform calibration measurements with known gas concentrations. As is discussed in Sect. 4.1.1, this is also a standard approach in open path TDLAS measurements where the distance is known. As mentioned there, a calibration against known concentrations has the advantage that the absorption cross section can be unknown, and it follows that L_{gas} (which is not an average but a single value in straight-path measurements), in principle also can be unknown.

Eq. (4.1), shows that $\langle L_{\mathrm{gas}} \rangle$ can be calculated from a calibration measurement according to

$$
\begin{aligned}
\langle L_{\mathrm{gas}} \rangle_{\mathrm{cal}} &= \ln \left(\frac{I}{I_0} \right)_{\mathrm{cal}} / (-\sigma c_{\mathrm{cal}}) \\
&= A_{\mathrm{cal}} / (-\sigma c_{\mathrm{cal}}).
\end{aligned} \tag{5.1}
$$

Here, $c_{\mathrm{cal.}}$ is the gas concentration in the calibration measurement and $A_{\mathrm{cal.}}$ is the absorbance.

For the approach to be successful the average path lengths in the calibration measurement and "evaluation measurement" must be similar, i.e.,

$$
\langle L_{\mathrm{gas}} \rangle_{\mathrm{cal}} \approx \langle L_{\mathrm{gas}} \rangle_{\mathrm{eval}}. \tag{5.2}
$$

The concentration in the evaluation measurement can then be calculated from the absorbance as

$$
\begin{aligned}
c_{\mathrm{eval}} &\approx A_{\mathrm{eval}} / (-\sigma \langle L_{\mathrm{gas}} \rangle_{\mathrm{cal}}) \\
&= c_{\mathrm{cal}} \times \frac{A_{\mathrm{eval}}}{A_{\mathrm{cal}}}.
\end{aligned} \tag{5.3}
$$

Clearly, the validity of Eq. (5.2) is crucial and this approach can thus only be used in situations when the geometries for the calibration and evaluation measurements are very similar. An example of where this approach is often useful is measurements on food packages, as was the case in Paper **V**. The mass-produced packages are usually very similar in shape, and a calibration measurement on a package with a known concentration is often valid for other packages of the same type. An example of a problem in this case can be when the amount of liquid varies greatly between packages, leading to a variation of the head-space volume.

Another example which belongs to this class of calibration, is dynamic measurements. In many situations, it is the time variation of a concentration which is important. In some cases the absolute concentration might be of no interest, and in others the concentration might be known at the beginning or end of the dynamic process. A specific example is measurements of gas diffusion between objects, with the main goal to find diffusion time constants [2, 111–114]. The work in Paper **XI** is also closely related to diffusion.

In biomedical applications of GASMAS, however, this calibration approach is seldom useful for quantitative concentration measurements, because of the strong geometrical differences between measurement objects.

5.2.2   Path length calibration with bulk methods

Another approach, which could provide knowledge of $\langle L_{\text{gas}} \rangle$, is to measure the total average optical[2] path length $\langle L_{\text{tot}} \rangle$, which includes the path through both the gas and the bulk/matrix material. Although the total path length is not useful in the Beer-Lambert law, in some cases there may exist knowledge on the relationship (or ratio) between $\langle L_{\text{gas}} \rangle$ and $\langle L_{\text{tot}} \rangle$. One especially simple example of this is when $\langle L_{\text{gas}} \rangle$ actually composes the very major part of $\langle L_{\text{tot}} \rangle$. This could be the case when the measurement object is made up by a large cavity surrounded by a thin layer of scattering material. Another example might be a "quasi-homogeneous" material, composed of a porous material with an even distribution of pores. In this case there may be a known ratio between $\langle L_{\text{gas}} \rangle$ and $\langle L_{\text{tot}} \rangle$, which could be obtained, e.g., through a calibration measurement. Three example techniques for measuring $\langle L_{\text{tot}} \rangle$ are briefly presented: "Time-of-flight spectroscopy", "Frequency-domain photon-migration" and "Frequency modulated light scattering interferometry". The latter was developed during the work in this thesis and will therefore be discussed in more detail.

[2] All methods to be presented in this section provide the optical distance, nL, where also the refractive index must be considered.

Time-of-flight spectroscopy

Photon time-of-flight spectroscopy (pTOFS), also referred to as time-resolved-spectroscopy (TRS), is a general method for analysis of light scattering materials. The tool is heavily employed, for example in characterization of biological tissue or pharmaceutical products [115, 116]. The biomedical applications include brain monitoring [117, 118], optical mammography [119–121], and in aiding photodynamic therapy for prostate cancer treatment [122].

The fundamental principle of pTOFS is to inject a very short laser pulse into the object under investigation, and thereafter measure the time-distribution of the light escaping the object at a position some distance from the injection spot. Due to scattering of the photons in the material, the detected pulse will be much broader in time than the injected pulse. The statistical distribution of detection times, makes up the time-of-flight (TOF) curve. The shape of the TOF-curve can be used to determine the optical properties of the medium by using models of light propagation in turbid media [123]. An example simulation is presented in Fig. 5.3.

In combination with GASMAS, the main information of interest provided by TOFS is the mean time-of-flight (MTOF). The MTOF is related to the mean light path length, $\langle L_{tot} \rangle$ through the average refractive index of the material. TOFS can thus be used to obtain $\langle L_{tot} \rangle$ in a GASMAS measurement.

As indicated, TOFS is a well-established and very powerful method. The combination with GASMAS is, however, unfortunately limited. The reason is the large technical differences between the two techniques. GASMAS is based in the use of narrowband, tunable diode lasers and large-area photo-diodes. TOFS, on the other hand, requires short light pulses (usually ps) which, through the Fourier transform are inherently broad band. The detection electronics in TOFS is usually based on so-called time-correlated single photon counting (TCSPC) [124], widely different from the GASMAS electronics. Any practical combination of these techniques, thus requires two separate setups, where measurements are performed on the same sample sequentially [125].

Frequency-domain photon-migration

An alternative to TOFS, which also has found a great field of applications, is the frequency-domain photon migration technique (FDPM). FDPM is also used for assessing the optical properties of diffuse media, such as biological tissue [126]. In the same way as for TOFS, FDPM is based on measuring time-delays of photons injected at one spot and detected at another. However, in FDPM, the injection is not a short laser pulse, but instead a continuous, intensity modulated wave of light. Because of the time-delays due to heavy internal scattering and absorption, the detected wave-
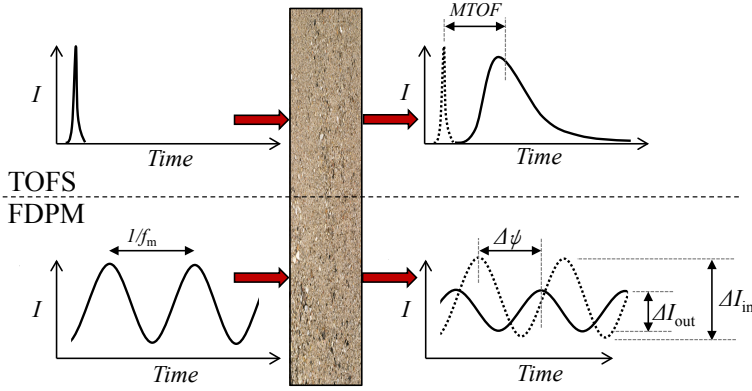
Figure 5.4. *The principles of TOFS and FDPM.*

form will be phase shifted (by $\Delta\psi$) and have a lower intensity modulation amplitude. Fig. 5.4 shows an illustration of the basic principles of TOFS and FDPM in a transmission measurement geometry. To be able to observe any phase shifts, the modulation frequency, f_{m}, must be sufficiently high. At relatively low modulation frequencies, Eq. (5.4) can approximate the phase shift as a function of mean optical path length, $\langle L_{\mathrm{tot}}\rangle$.

$$\Delta\psi = 2\pi f_{\mathrm{m}} \left\langle L_{\mathrm{tot}}\right\rangle / c_0 \tag{5.4}$$

The validity of the equation is decreased as the scattering and modulation frequency increase. In practice, to characterize the optical properties of a sample, the modulation frequency is often varied, and the phase shift and demodulation are found as functions of the modulation frequency [127]. The exact relation between the shape of the detected waveform and $\langle L_{\mathrm{tot}}\rangle$ may be found by reference measurements and theoretical fitting. To obtain resolutions in the millimeter regime, modulation frequencies in the order of hundreds of MHz are used. Although these relatively high frequencies are needed, this is something which is quite readily achieved with RF components and the distributed feedback (DFB) lasers typically employed by GASMAS. The main drawback in the combination of GASMAS and FDPM today is the need for frequent calibration of the phase shift. The reason is that the system itself also introduces a phase shift, which depends on the received intensity, and which drifts with time.
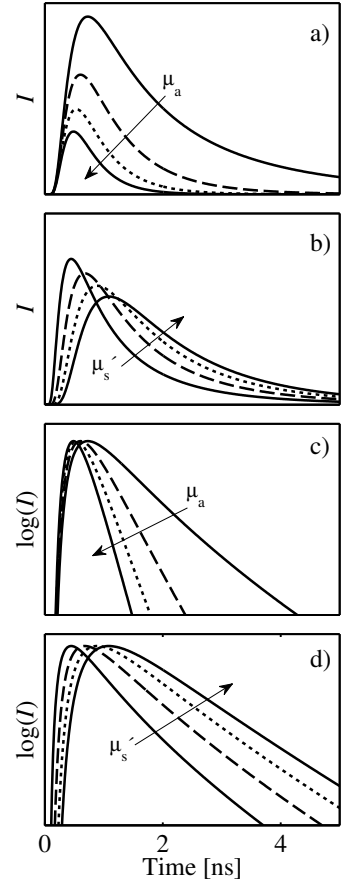
Figure 5.3. *Simulations of the resulting light fluence (intensity, I, used on axes) 2 cm away from an injection point in an infinite medium, using the diffusion approximation [123]. An infinitely short, isotropic pulse has been injected while μ_{a} and μ_{s}' (the absorption- and reduced scattering coefficient, respectively) are changed. a) μ_{s}' is kept fixed at 8 cm^{-1} while μ_{a} is varied according to $\mu_{\mathrm{a}} = [0.01, 0.04, 0.07, 0.10]$ cm^{-1}. b) μ_{a} is kept fixed at 0.02 cm^{-1} while μ_{s}' is varied according to $\mu_{\mathrm{s}}' = [5, 8, 11, 14]$ cm^{-1}. c) and d) show the logarithms of the data in a) and b), respectively. By looking at the logarithms it is clear how μ_{a} is mainly affecting the slope of the late part of the curve, while μ_{s}' is mainly affecting the peak position (the time of maximum intensity).*

Frequency modulated light scattering interferometry

The technique FMCW, as used for ranging in, e.g., optical fibers, was briefly introduced in Sect. 4.2. In the original methods, one, or possibly a few, distinct distances/path lengths/delays are searched for and found by the heterodyne beating between a reference and a signal beam. In principle, however, there are no theoretical limitation on using the same technique for finding a distribution of delays. In this case, there will not be one distinct beat frequency but rather a spectrum of frequencies which can be obtained by the Fourier transform of the interference signal. This variety of the technique working in the diffuse regime was first proposed in Paper **VI** and has later been used in Papers **VII** and **VIII**, as well as in Refs [128, 129].

The principle of the optical variety of FMCW is that a wavelength tunable diode laser is ramped in wavelength and the beam is split in two parts; see Fig. 5.5a. One part is sent to a light detector through a well-defined path – this is referred to as the reference beam. (In the figure, the chosen setup is a Michelson interferometer.) The other part of the beam – the sample beam – is sent to a sample, in which the light will travel an unknown path length and thus acquire an unknown delay, τ, compared to the reference beam. The light emerging from the sample will have a slightly different frequency/wavelength than the reference, due to the fact that the source is wavelength ramped and due to the different delays in the reference and sample beams. The emerging sample light is sent to the same detector as the reference beam. If the two beams are combined in such a way that they can interfere (coming in the same direction and to the same area), their slightly different frequencies will induce a beating (oscillating light intensity) which is picked up by the detection system. The frequency of the oscillation, f_b, gives the optical path length in the sample (or rather, the optical path length difference between the sample and reference) according to Eq. (5.5), which is repeated here: [3]

[3] n is the refractive index, L is the path length, f_{scan} is the scanning frequency, $\Delta\nu$ is the range of frequencies scanned and c_0 is the speed of light in vacuum.

$$f_b = 2nR f_{scan} \Delta\nu / c_0 \qquad (5.5)$$

To discriminate the variety of FMCW working in the diffuse light regime from the "discrete" method, the diffuse approach has lately been given the name *Frequency modulated light scattering interferometry*, FMLSI. The principle of FMLSI is shown in Fig. 5.5b, and is basically the same as for FMCW. In the schematics, a Mach-Zehnder interferometer is used where the heavy light scattering in the sample induces delays of the sample photons. The reference beam still consists of a ramped signal with a single frequency at any one time, while the sample beam will have a distribution of frequencies. The beating will thus consist of a distribution of beat frequencies. By applying Eq. (5.6), the

Figure 5.5. *The principles of a) "discrete" (only single discrete delays) FMCW and b) FMLSI, working in the diffuse light regime. Dashed lines represent the reference wave while the solid and "smeared" lines represent the sample waves in the discrete and diffuse cases, respectively. The beat frequencies that are drawn negative indicate their opposite phases. Note that the range of interest or the fully operating range "r_o" of FMLSI is much shorter in the figure compared to the real case, where the sweep time is much longer than the delays.*

power spectrum of the detected signal provides the equivalence to the corresponding time-of-flight distribution.

$$\bar{\tau} + \tau_0 = f_{\mathrm{b}}/\left(f_{\mathrm{scan}}\Delta\nu\right) \tag{5.6}$$

Here, τ_0 is the offset path length difference between the sample and reference paths, and $\bar{\tau}$ is the distribution of delay times, corresponding to the times-of-flight given by TOFS.

Due to the extremely high frequency of optical light, $\Delta\nu$ can easily be quite a large number – DFB diode lasers can often be tuned over a hundred GHz. Assuming $\Delta\nu = 100$ GHz, $f_{\mathrm{scan}} = 10$ Hz, and $\langle n \rangle = 1.5$, a 10 mm path length difference would give $f_{\mathrm{b}} = 50$ Hz. The beat frequency resolution in the final power spectrum, together with the tuning range and scanning frequency, set the limit for the time delay resolution. The beat frequency resolution, following from the discrete fast Fourier transform, is inversely proportional to r_{o} in Fig. 5.5b. Increasing f_{scan} means a shorter integration time, which leads to the cancellation of its practical effect on the delay resolution. To improve resolution, the tuning range must therefore be increased. Since quite low scanning frequencies can be employed, it is attractive to use external cavity

Figure 5.6. *The method of path length calibration with another gas of known concentration is based on injecting light of two center wavelengths, λ_1 and λ_2, into the sample and assumes that they experience the same average path length through gas.*
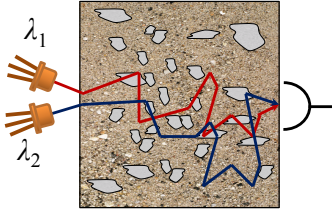
diode lasers (ECDLs), which can have tuning ranges of several nm. The SNR of the technique is heavily dependent on the light intensity. At this stage, it is hard to obtain the same signal quality as with TOFS and FDPM.

5.2.3 Path length calibration with another gas of known concentration

An approach for finding $\langle L_{gas} \rangle$ that has been extensively used in GASMAS is to probe a gas for which the concentration is known, at the same time as the gas of unknown concentration. The fundamental assumption is then that the light probing the two gases experience the same $\langle L_{gas} \rangle$. The motivation for the validity of this assumption is that the bulk optical properties (mainly μ_s' and μ_a) change slowly with wavelength so that they are similar for the two wavelengths used. The approach was first introduced in [112] and has since been used in several GASMAS studies; see Refs [77, 111], as well as Papers **IV** and **V**.

Fig. 5.6 shows an illustration of the traces by one individual photon of each of two wavelengths injected into a sample and detected at the opposite side. The path of each photon is random but the statistical average of the photon path lengths, $\langle L_{gas} \rangle$ and $\langle L_{tot} \rangle$, are assumed to be similar for the two wavelengths. In this case, the following calculation can be performed:

$$\langle L_{gas} \rangle_k = A_k / (-\sigma_k c_k)$$
$$\Rightarrow \left[\langle L_{gas} \rangle_k \approx \langle L_{gas} \rangle_{uk} \right]$$
$$\Rightarrow c_{uk} \approx A_{uk} / (\langle L_{gas} \rangle_k \sigma_{uk}) \tag{5.7}$$

Here the subscript "k" indicates the gas of known concentration while "uk" indicates the gas of unknown concentration.

In practice, the only gas so far used as "gas of known concentration" is water vapor, which has been sensed at around 935 and 980 nm, and has been used for calibrating the path length for oxygen sensing at around 760 nm. The reason why water vapor is especially suitable for the task is that, as long as the temperature is known, and liquid water is present in a relatively closed environment, the water vapor concentration can be calculated, for example, with the Arden-Buck equation [130].

$$c_{H_2O} = 6.032 \times 10^{-3} e^{17.502T/(240.97+T)} \tag{5.8}$$

Here, T is the temperature in $^\circ$C and c_{H_2O} is the concentration [% by volume] of water vapor.

5.2.4   Path length independent measurements

A GASMAS approach that is completely different from the ones presented above is trying to circumvent knowing $\langle L_{gas} \rangle$, and still obtain quantitative gas concentrations. This might at first seem like a utopian idea, but it is actually a reasonable notion which is based on the physics introduced in Sect. 3.1.3. One of the conclusions there is that the lineshape of a gaseous absorption line is dependent not only on the temperature and absolute pressure of the gas environment, but also its molecular composition. The normalized lineshape function of a given absorption line, $\bar{\chi}(\lambda)$,[4] can therefore be written

$$\bar{\chi}(\nu)_i = F(T, P_i, P_{i+1}, ..., P_N). \qquad (5.9)$$

Here, $\bar{\chi}(\nu)_i$ is the lineshape for molecular species i, T is the temperature, and P_i to P_N are the partial pressures of the individual neighbor molecular species, i to N (including the species measured, i). On top of this $\bar{\chi}(\nu))$ depends on other external factors, such as wall collision effects in the case of very small pores or cavities [131–135], as was predicted to be relevant for GASMAS already in the first publication in the field [105]. However, this is not an aspect relevant for the work of this thesis.

Thanks to the above, it is possible to find the concentration of a certain species, $i+1$, by measuring the lineshape of an absorption line of another molecular species i, as long as they are present in the same gas mixture.

This approach for performing quantitative gas concentration measurements was introduced in Paper **IX**. In this paper, the concentrations of gaseous oxygen and nitrogen were measured using an absorption line of water vapor at around 935 nm (vibration: $(v_1, v_2, v_3) = (000) \rightarrow (201)$; rotation: $(J, K_a, K_c) = (303) \rightarrow (404)$). These measurements were actually performed with the gas mixture in a gas cell for easy and rapid gas changes. The recorded absorption spectra were, however, normalized before further analysis and the fact that the light followed a straight path in these measurements is not relevant.[5]

To be sensitive to small changes of neighbor gas concentrations, it is important (i) to have a high quality of the absorption spectrum, so that its shape can be carefully analyzed, and (ii) that the effect on the lineshape by the molecule of interest (the molecule whose concentration is sought for) is large enough and sufficiently different from other neighbor molecules. It is thus important to find an absorption line for which γ_{ij} (the line broadening coefficient for broadening of a line belonging to species i, by a neighboring molecule j) and δ_{ij} (the corresponding line shift coefficient) are as different as possible for the involved neighbor species. Note that, if P and T are known, it would (assuming the lineshape is solely

[4] Or written as a function of wavelength, $\bar{\chi}(\lambda)$.

[5] This was in the small absorption range where $e^{-x} \approx 1 - x$. In this range, the distribution of path lengths in the GASMAS case does not affect the lineshape.
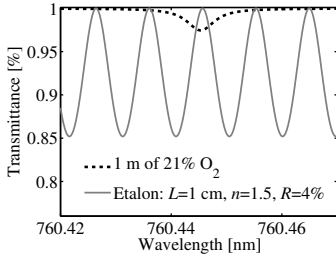
Figure 5.7. *The transmission through an etalon together with the transmission of oxygen in the same region. Since the width of the absorption line is in the same order as the FSR of the etalon, the separation between the two effects becomes especially difficult.*

described by its width and shift) be possible to calculate the concentrations of three molecular species, if these are the only ones present, i.e. if $N = 3$. We then have a system of equations with three unknowns, c_1, c_2 and c_3. If we measure two quantities, γ_{tot} and δ_{tot}, and know that $c_1 + c_2 + c_3 = 1$, we find:

$$\gamma_{tot} = c_1\gamma_1 + c_2\gamma_2 + c_3\gamma_3$$
$$\delta_{tot} = c_1\delta_1 + c_2\delta_2 + c_3\delta_3$$
$$1 = c_1 + c_2 + c_3. \tag{5.10}$$

So far unpublished data, using a stronger absorption line of water vapor, at 1392 nm, simultaneously gave the concentrations of CO_2, N_2 and O_2 with good accuracies (the concentration of the water vapor itself was known).

To obtain the actual concentrations, the data analysis approach has up to now been based on the computational methods of principal component analysis (PCA) and linear regression models. These models will not be discussed here and the reader is referred to Refs [63, 136, 137] for a comprehensive literature.

5.3 Coping with interference fringes

Another "problem" that GASMAS [138] must cope with, as well as TDLAS in general [139, 140], is the influence of optical interferences in the spectroscopic light. Because of the large significance this problem can acquire in a GASMAS measurement, a small section discussing the subject is motivated.

The typical example of interference fringes is the spectral scanning of a Fabry-Pérot etalon, which in its simplest form consists of a piece of glass with very planar and parallel surfaces. Due to the interference between the waves that have been internally reflected different numbers of times, some wavelengths will be transmitted more than others. The wavelength or frequency separation between wavelengths with maximum transmission is given by the free spectral range (FRS) of the etalon; see Eq. (5.11).

$$\Delta\nu = c/(2nL)$$
$$\Delta\lambda = \lambda^2/(2nL) \tag{5.11}$$

Here $\Delta\nu$ is the FSR in optical frequency and $\Delta\lambda$ is the FSR in wavelength. The higher the finesse of the etalon, the larger the difference between the maximum and minimum transmission, and the sharper the transmission peaks become. Fig. 5.7 gives an example of the transmission of a 1 cm etalon made of standard glass together with the transmission through 1 m of air, in a wavelength

region where oxygen has an absorption line. The figure demonstrates the nature of the problem with these fringes – they will, in a similar way to absorption lines, induce a wavelength dependent transmission. To separate these two effects from each other is sometimes very difficult, especially if the FSR is similar to the width of the absorption line.

Further, averaging the signal will generally not reduce this "artifact", as it does for other types of noise, as long as the physical geometry of the measurement system and sample is static. In GASMAS, a measured signal generally contains fringes originating from the system optics (collimating lenses, optical fibers, etc.), as well as from the measured sample.

Two main approaches have been used for reducing fringes in GASMAS measurements: (**i**) To induce time dependent changes of the fringes by vibrating the sample and/or system, and (**ii**) to try to separately and simultaneously measure the system transmission, containing most of the fringes. Usually both approaches are used in combination. Fig. 5.8 gives an example of when approach (**i**) was used. The improvement of the signal quality when vibrating the laser in a measurement of oxygen in a juice bottle headspace is clear.

The method for implementing approach (**ii**) has often been to split the light from an optical fiber, guiding the laser light into two parts: one going to the sample (e.g., ∼90%) and the rest going to a reference detector where no gas absorption is present. The latter is then measuring the transmission without gas absorption and the former the transmission with absorption. The difference should, in the ideal case, represent the pure gas absorption spectrum. This method is often referred to as *balanced detection* [141]. This approach has proven very powerful but has two clear drawbacks – the additional optical component for splitting the light can potentially induce new fringes, and only the fringes that are common to the two arms can be removed. Thus no fringes induced after the light splitting can be handled. A slightly modified version of (**ii**) was therefore implemented during the work in this thesis. The reference detector was now put directly on the sample, but close to the light injection point; see Fig. 5.9a. As the detector is placed close to the injection point, the light detected by that detector can in many cases be considered as not having passed through any gas, while still carrying most of the fringe information. The approach was used in Paper **XVII** and an example of its effectiveness is seen in Fig. 5.9b.

5.4 Applications of GASMAS

Since its invention in 2001 [105] the GASMAS technique has been applied to measure gases located inside a large number of turbid
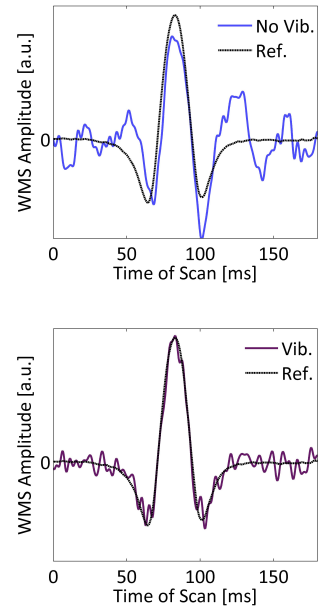
Figure 5.8. *An example of how vibrations can improve the signal quality. The example is taken from a recording of oxygen through the headspace of a juice package. A small cell phone vibrator is vibrating the laser mount during the lower measurement while this is turned off in the upper measurement. A long-path (∼1 m) reference recording is included as an example of a perfect WMS curve.*
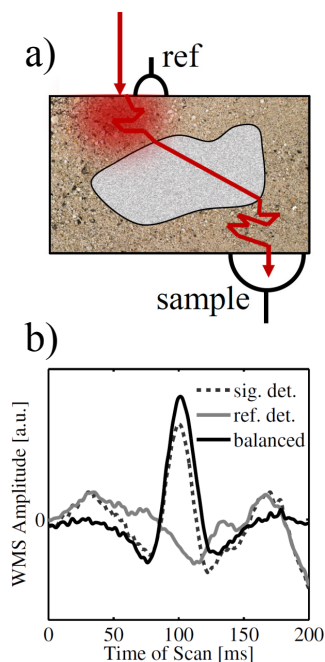
Figure 5.9. *a) Schematic of the implementation of balanced detection by using a small reference photo-diode close to the illumination point. b) An example of how balanced detection can improve the signal quality. The example is taken from one of the intestine signals in Paper **XVII**. It is obvious how part of the signal structure is existing also in the recording by the reference detector, indicating that this is due to common interference fringes. When this structure is removed the signal quality is greatly improved.*

samples, as well as for determining other properties of the materials. Furthermore, the possibility of using materials with strong light scattering proprieties but still with low bulk absorption as miniature multipass absorption "cells" has been extensively studied.

- Oxygen and water vapor in wood has been measured where gas diffusion and fiber orientation dependencies were investigated, as well as wood drying processes in Refs [114, 142].

- Oxygen and water vapor in human sinus cavities have been studied in Refs [77, 79, 112, 143, 144]. Clinical trials at a hospital were performed.

- A feasibility study was performed to investigate the possibilities for measurements of gas in human lungs in Ref. [145]. The study involved measurements on a tissue phantom as well as on a wild boar lung.

- Pharmaceutical tablets have been studied in Refs [146, 147], and nanoporous ceramic samples in Refs [131–135, 148]. The nanoporous samples are examples of materials where the path length can be prolonged up to 750 times the thickness of the sample [148], and which therefore form feasible alternatives to alignment sensitive multipass cells. Line broadening due to wall-collisions is also scrutinized in these studies.

- Food and food packages have been investigated in Refs [105, 111, 113].

5.4.1 Applications addressed in this thesis

The applications investigated in the work of this thesis are in the fields of food and food packaging, wood characterization, and studies of gas in the lungs and intestines of humans. Brief descriptions of the studies are included below.

In Paper **XI** the absolute pressure of the gas in the pores of apple tissue was investigated in connection with vacuum impregnation of the apple pieces. To our surprise, the decreased internal pore pressure due the impregnation was retained for a timescale of hours during measurements (after the pieces had been exposed to ambient pressure). The gas pressures were estimated through analysis of the widths of the pressure broadened lines.

In Paper **X** the GASMAS technique was applied to wood in combination with pTOFS (or TRS) to extract information regarding porosity, moisture content, gas permeability, chemical composition and anisotropy. Of these properties, GASMAS mainly contributed to finding the gas permeability and the porosity.

In Paper **IV** the oxygen concentrations in a large set of juice packages with modified atmospheres were investigated. The paper

thus presents the first laser spectroscopic gas studies on packages with MAs. Three batches with different expiration dates were investigated, with 20 packages in each batch. A distinct difference in the oxygen concentration between the batches was found. Paper **V** further scrutinizes the performance of GASMAS for measurements of the headspace gas composition in beverage packages. The results from the spectroscopic measurements were compared with those from an intrusive reference sensor based on gas extraction.

Paper **XVII** presents the first *in vivo* measurements for studies of the gas in the lungs and intestines of three full-term newborn babies. The gas in the intestines was relatively simple to measure while the lungs (which are covered by thicker tissue) pose a greater challenge. It was possible to measure water vapor, but not oxygen.

FLUORESCENCE LIGHT DETECTION AND RANGING FOR ANIMAL ECOLOGY APPLICATIONS

As discussed in Sect. 2.3, the methods generally employed for remote classification of both flying insects and birds give limited information. An option for remote insect detection is to employ the LIDAR technique [149]. An interesting alternative which could be used for classification is based on measuring the modulation in an elastic CW LIDAR return due to the wing-beats of the animals [150, 151]. In this chapter, our approaches using LIF-LIDAR (Sect. 4.3.1) for detection and classification of insects and birds are introduced.

6.1 Remote sensing of damselflies

As mentioned in Sect. 2.3.1, a common way to perform migration studies of damselflies and other insects is to mark captured individuals with colored liquid dyes, or with powders, and then see how these individuals spread into neighboring habitats. Many of the powders used are extremely fluorescent, with a fluorescence spectrum matching the color of the substance. To use this property of the dyes in combination with LIF-LIDAR, is thus an attractive alternative to the currently employed methods, which often include re-capture of the same individuals. In this way, a number of individuals can be marked with differently colored powders, discriminating between, e.g., species and sexes. A LIF-LIDAR system can be positioned in the same habitat or elsewhere to automatically count the number of individuals in the different groups passing through the laser-beam as a function of time after release (usu-

Figure 6.2. *Schematic setup for the multi-channel LIF-LIDAR used in the field for the measurements on damselflies (Paper **XIII**). P=polarizer, LP=long-pass filter, SP=short-pass filter, D=dichroic beam-splitter, M=mirror, UV-M=UV-mirror. In some experiments the received light was instead sent to an image intensified spectrometer, through a fiber positioned a the telescope focus.*

Figure 6.1. *Two damselflies marked with blue and orange powders, respectively.*

ally several days). The approach allows for automatic collection of large sample statistics, and the possibility of being completely unmanned.

Apart for the possibilities of marking the damselflies, it is also possible to use their natural auto-fluorescence for discrimination with a LIF-LIDAR system. The observed colors of damselflies are composed of both chemical imprints as well as structural colors (interference based colors) [152, 153]. The chemical imprints come from chitin and melanin which peak in absorption at a wavelength around 330 nm. The structural colors are mainly due to an arrangement of nano-spheres with sizes around 100 nm [152]. Depending on the size and arrangement of these spheres, as well as on the angles of observation and illumination, the reflectance spectrum which has features around 100 nm wide, will move between blue and green. When employing LIF-LIDAR, it is the structural and chemical transmittance of the fluorescence induced mainly in the chitin, which is observed. However, the lower fluorescence yield, together with the broader structures of the emitted auto-fluorescence when compared to that of the artificial powders, make LIF-based discrimination and classification more challenging without marking.

Ref. [153] describes the first feasibility study of using LIF-

LIDAR for remote classification of damselflies. Paper **XIII** continues that study (in which laboratory measurements were carried out) by performing the first measurements in the field. The location for the experiments was a river in Southern Sweden. In these experiments, the illumination wavelength was 355 nm and three detection channels were used – depolarized elastic back-scattering, and two fluorescence channels. A schematic figure of this setup is seen in Fig. 6.2.

During the experiments for Paper **XIII** a group of starlings happened to pass through the beam – resulting in huge fluorescence signals unintentionally being recorded. Seeing these signals, it was hard to avoid investigating further if the LIF-LIDAR approach could also be used for remote bird classification.

6.2   Remote sensing of birds

Following the starling event during the insect measurements, experiments were performed to evaluate the possibilities for using LIF-LIDAR also for bird classification. The first study of this kind is presented in Paper **XIV**. This study involved laboratory measurements of the fluorescence spectra of 26 bird species, obtained on museum samples with excitation at multiple UV wavelengths. Test range LIF-LIDAR measurements at a distance of 60 m were performed with excitation at 266 and 355 nm. Essentially the same setup as in Fig. 6.2 was used.

Paper **XV** presents the first measurements performed in field, at the Kullaberg nature reserve in Southwest Sweden. To ensure the birds' eye-safety, and to allow for an extra fluorescence channel in the UV region, the illumination wavelength was in this study held at 266 nm. Fig. 6.3 shows remotely measured fluorescence spectra of six museum bird species. The transmittance of the three fluorescence channels used in this study are included. By integrating the spectral channel transmissions multiplied by the spectra of the birds, the position of each bird in the 3D-space spanned by the three fluorescence channels, can be determined, as seen in the bottom part of the figure.

In the same study, a variety of other remote sensing methods were also used, including passive, thermal infrared imaging. In this case the interference based transmittance as a function of wing angle is investigated.

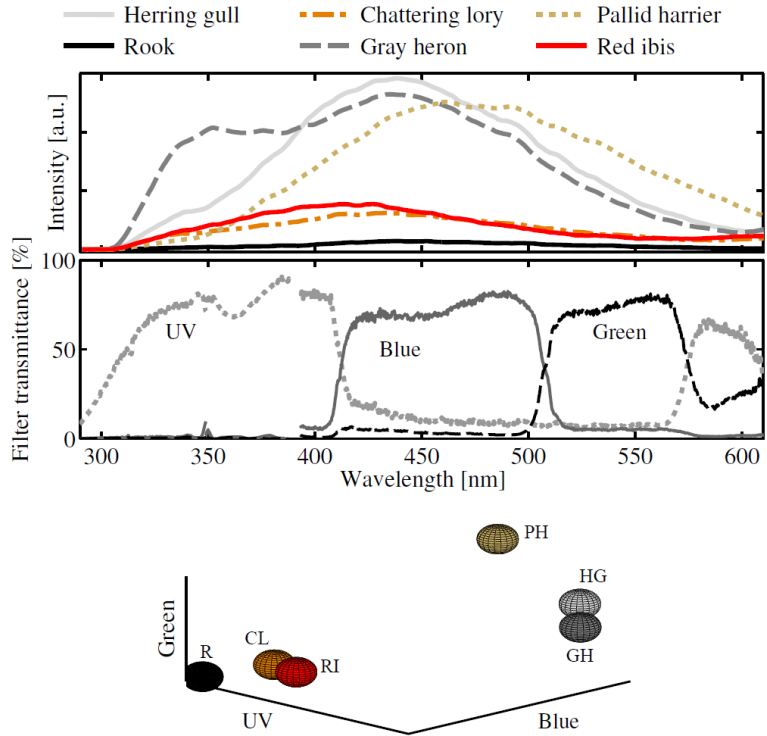**Figure 6.3.** **Top**: *Remote fluorescence spectra of six museum bird species obtained at a distance of 60 m.* **Middle**: *Three broad-band fluorescence channels created by a combination of beam splitters and optical filters.* **Bottom**: *The positions of the six included spectra in the 3D-space created by the three fluorescence channels. The abbreviated names of the six birds are included.*

Conclusion and perspectives

Differential absorption LIDAR is a key technique for trace gas studies in the atmosphere. In this thesis, it was, for the first time, applied with the aim of measuring glyoxal. Although, the low concentrations of the gas at the location in Sweden prevented its detection, it should form an important tool at places with a higher concentration. This is also true for DIAL measurements of mercury. A study in this thesis presents the first mercury DIAL measurements performed in China. As a result of the strong collaboration between the Swedish group and Chinese colleagues, a state of the art LIDAR system is currently being constructed in China, where environmental monitoring may be especially important.

The work within the field of animal ecology is based on applying the long-established LIF-LIDAR methods, to novel applications in bird and insect migration studies. The main system used for these studies, was the very versatile Lund mobile LIDAR system, housed in a heavy truck weighing several tons. The power needed for the system was delivered in the field by a 40 kW Diesel power supply. Furthermore, the operation of the system needs constant tweaking and optimization procedures. This type of system is clearly not what the ecologists would finally like to use. However, when a final application is aimed for, the system complexity could be reduced greatly, and unmanned operation may be possible. In fact, work following the articles in the thesis has applied much simpler techniques and has demonstrated great potenital for remote animal classification. As a continuation of this thesis work, a system devoted for ecological use was developed (mainly by Dr. Mikkel Brydegaard), called LUMBO (Lund University Mobile Biosphere Observatory). This system is now a part of the Centre for Animal Movement Research in Lund.

The technique GASMAS is applying the well-developed methods of WM-TDLAS, in the new field of gas sensing in scattering media. Most of the work in the GASMAS field is thus concerned

with how to cope with the special problems arising in these applications. Although this technique transfer was started in 2001, the technique should probably still be considered as being in its early stages. The potential for this type of measurements seems enormous, although many practical limitations are still present. One of these limitations is the unknown optical path length, which generally prevents quantitative gas concentration measurements. Much of the work in the thesis was devoted to solving this problem, and many potential solutions were developed. The newest approaches to path length independent measurements will probably stay at the research level for some time to come. If the signal quality can be improved further, this approach could hopefully be of real use. Follow-up studies not included in the thesis also show how multiple gases can be measured simultaneously with the technique. The other approach presented to solve the path length problem was aimed at developing methods which can measure the total light path length, and which can readily be combined with the technical platform of GASMAS. Although the practical use of the latter approach is limited to samples with a known relationship between the path length through the bulk material and through the gas, there are many cases where it may be applicable. One example is food packaging, where the headspace often constitutes the major distance.

Very applied GASMAS studies were presented for medical diagnosis, wood characterization, analysis of food packages, and for pressure measurements in fruit.

The work regarding the lung and intestine status of infants is still in its very early stages. The study included in the thesis showed successful measurements for water vapor, but not for oxygen, in the lungs of three full-term infants. Clearly, oxygen signals are needed for there to be any chance of taking the technique forward to clinically relevant studies. In fact, a large study on around thirty infants, following the one included in the thesis, was recently performed at the Skåne University Hospital. Although the data analysis is still ongoing, it is already a fact that oxygen signals were retrieved. More measurements, which aim at helping premature infants in their early stages, are planned.

Both GASMAS measurements and time-resolved spectroscopy have been performed on wood before, but we have now applied these techniques in combination. The combination allows for extraction of many parameters regarding gas permeability, porosity, chemical composition and anisotropy. A future goal is to apply this technique combination to water logged wood for assessing its preservation status.

The food package application of GASMAS is, together with measurements on human sinus cavities, probably the one that is most developed. The studies in this area have now reached a level where it is possible to commercialize the technique.

COMMENTS ON THE PAPERS

I **Active feedback regulation of a Michelson interferometer to achieve zero-background absorption measurements**
The paper presents a way to improve a newly suggested technique for performing gas absorption measurements in a darkfield, or zero-background, environment, using an interferometer. The improvement lies in stabilizing the interferometer in the destructive interference position, using a piezo element and a PID controller. The initial idea for the work came from Guan through an earlier study. Guan, Svanberg and I planned the experiments, while I performed a major part of the experiments, data analysis and manuscript preparation. Technical assistance by Guan was invaluable.

II **Vertical lidar sounding of atomic mercury and nitric oxide in a major Chinese city**
Differential absorption LIDAR was employed, using the Lund LIDAR system, to measure the pollutant gases atomic mercury and nitric oxide. Horizontal and vertical measurements were performed, and diurnal variations of gas distributions were studied. I contributed to the planning and execution of the measurements while Guan was the main person responsible for setting up and managing the LIDAR system. I had a minor role in the data analysis, while contributing more to the manuscript preparation.

III **First attempt to monitor atmospheric glyoxal using differential absorption lidar**
This paper presents the first measurements employing differential absorption LIDAR to measure glyoxal in the atmosphere. Apart from this trace gas, nitrogen dioxide was also measured, mainly to know its impact on the glyoxal results. The low concentration of glyoxal during the measurements performed in Sweden was under the detection limit of the system employed. The planning of this experiment was a group effort with inputs by Greek and Swedish researchers. I took part in this planning, as well as in the measurements. The data analysis was mainly performed by Mei, while I made more contributions to the manuscript draft.

IV **Non-intrusive measurements of headspace gas composition in liquid food packages made of translucent materials**
The paper presents a study where the oxygen concentrations in a large set of juice containers are measured with laser spectroscopy. Shelf-time dependent processes were observed. I took part in preparatory discussions and the execution of the measurements and data analysis, as well as contributing to the figure preparation and manuscript writing. Lewander was the main person responsible for the study.

V **Non-intrusive headspace gas measurements by laser spectroscopy – Performance validation by a reference sensor**
This paper is a validation of GASMAS for measuring the oxygen concentration in non-transparent beverage containers. The initiative for, and the planning of the experiments came through discussions with all authors. I performed most of the measurements together with Cocola, analyzed the data, prepared all figures and wrote a major part of the manuscript draft.

VI **Assessment of photon migration in scattering media using heterodyning techniques with a frequency modulated diode laser**

The paper presents the first photon migration measurements in diffusive materials using the frequency-modulated continuous-wave technique, adopted from the telecommunication field. Guan initiated the introduction of the technique into our field and was the key person for planning and executing the experiments. I contributed to this planning together with Svanberg, performed part of the experiments and wrote parts of the manuscript.

VII **Gas spectroscopy and optical path-length assessment in scattering media using a frequency-modulated continuous-wave diode laser**

This paper presents a system combining gas absorption measurements and photon migration measurements, using the same diode laser. The frequency-modulated continuous-wave approach for evaluating photon migration enables this straightforward combination with gas spectroscopy, something which would be impossible with, e.g., photon time-of-flight spectroscopy. The work continues that in Paper **VI**. I took an active part in the planning and execution of the experiments, while Mei made the major contribution to the data analysis and manuscript preparation.

VIII **Characterization and validation of the frequency-modulated continuous-wave technique for assessment of photon migration in solid scattering media**

The paper validates the photon migration retrieval performance of the frequency-modulated continuous-wave technique, as a continuation of Papers **VI** and **VII**. Photon migration results are compared with those of the gold standard – photon time-of-flight spectroscopy – and a very good agreement is found. I took part in experimental discussions and work, and made minor contributions to the manuscript preparation, while Mei was leading the work.

IX **Laser spectroscopic gas concentration measurements in situations with unknown optical path length enabled by absorption line shape analysis**

The paper presents a completely new approach for determining gas concentrations. The absorption line shape of a measured gas is used to extract information about the concentrations of other gases in a mixture. While I had the idea for the new approach for gas concentration measurements, frequent discussion with other coauthors were very valuable. I performed most of the measurements, wrote most of the manuscript draft, and prepared all of the figures.

X **Diffuse optical techniques applied to wood characterisation**

The paper presents spectroscopic measurements on wood. GASMAS was used for pore gas measurements while time-resolved techniques were used for measuring the optical properties of the wood itself. The combination of these techniques provides much information about the chemical and physical properties of the wood. I took part in the planning of the experiments, together with all coauthors; made a minor contribution to the GASMAS measurements and analysis; and wrote minor parts of the manuscript. Bargigia was the key person for holding the different pieces of the work together.

XI **Gas in scattering media absorption spectroscopy (GASMAS) detected persistent vacuum in apple tissue after vacuum impregnation**

In this study, laser spectrocopy was used to evaluate the gas pressure in apple tissue after vacuum impregnation. To our surprise, the low pressure remained in the tissue for a timescale of hours during measurements. While Tylewicz managed the vacuum impregnation, Cocola and I were responsible for the spectroscopic measurements. I took part in the planning of the experiments with all coauthors, and contributed to figure preparation and manuscript writing.

XII **Tea classification and quality assessment using laser-induced fluorescence and chemometric evaluation**

The paper explores the possibility of using laser-induced fluorescence to evaluate the quality of tea leaves. A pulsed UV laser illuminated the tea, inducing fluorescence which was spectroscopically analyzed with singular value decomposition. A judgment by a panel of tea tasting experts was compared to the fluorescence method. I took part in experimental discussions and performed the measurements together with Mei. I made contributions to the manuscript writing, while Mei and Brydegaard performed most of the data analysis.

XIII **Insect monitoring with fluorescence lidar techniques: field experiments**

In this paper we report on the first attempts to use fluorescence LIDAR for insect detection and monitoring. Laboratory studies, as well as field measurements at a river site, were performed with good results. I took part in the planning and execution of the measurements, and wrote part of the manuscript draft. I had a minor role in the data analysis.

XIV **Feasibility study: fluorescence lidar for remote bird classification**

The paper presents the first fluorescence LIDAR measurements on birds. The start of this work was actually the study presented in Paper **XIII**, where a small flock of starlings happened to pass through the laser beam during insect measurements, inducing huge fluorescence signals. While Brydegaard took the main initiative to the work, I, together with all coauthors, took part in its planning. I contributed to most measurements and some data analysis, prepared some of the figures, and part of the manuscript text.

XV **Remote nocturnal bird classification by spectroscopy in extended wavelength ranges**
This paper presents results from a two week long field campaign, where a variety of techniques for remote bird classification were validated. The experiments used a combination of fluorescence LIDAR exciting in the UV, passive monitoring of scattered NIR sunlight, and IR-camera recording of the MIR radiation emitted by the birds. Brydegaard was the main driving force for the experiments and was the key person for making the combination of techniques work in parallel. I was responsible for setting up, managing, and presenting the LIDAR part of the experiments, and coordinating the writing of the manuscript. I wrote much of the text and prepared many of the figures.

XVI **Passive unmanned sky spectroscopy for remote bird classification**
This paper springs from the passive sunlight scattering part of Paper **XV**. A range of experiments were performed to evaluate the possibility of using the spectroscopic information in scattered sunlight for bird classification and altitude estimation. Brydegaard took the initiative to perform and execute the experiments, while much of the planning was conducted by all the coauthors. I performed most of the data analysis and writing of the manuscript.

XVII **Noninvasive monitoring of gas in the lungs and intestines of newborn infants using diode lasers: feasibility study**
This paper is the result of the first *in vivo*, laser spectroscopic measurements on the lungs and intestines of humans, following the work in a previous phantom study. Measurements of oxygen and water vapor were performed on three full-term infants. The planning of the experiments was performed between all authors. I performed most of the measurements, analyzed the data, wrote the technical part of the manuscript draft, and prepared most figures. Krite Svanberg took main responsibility for the medical aspects of the work.

Acknowledgements

It would clearly not have been possible to perform this work without help, and I would therefore like to thank a number of people.

First, I would like to thank my supervisors Sune Svanberg and Stefan Andersson-Engels. I am very grateful for the chance to be one of Sune's countless PhD students. It has been great to learn from your deep knowledge and enthusiasm. It is such a joy so see your hands-on approach to laboratory field work. Thank you, Stefan, for believing in my sometimes crazy ideas, but especially for first questioning them. Thank you also for giving the sort of "all-embracing" feedback on drafts that I would not have been able to think of myself. Thank you also for trying hard to get over-bridging communications started, by organizing topical meetings, but also by arranging group activities like Kayak paddling.

There are also a number of other group members who deserve gratitude. Katarina Svanberg – You are so knowledgeable and always very frank, no matter who you talk to – this is very uplifting. Gabriel Somesfalean – thank you for always proof reading manuscripts so carefully – this is often needed with my quickly scribbled ideas for papers. Mikkel Brydegaard – thank you for bringing some communistic spirit and fun into the office, and for not being afraid of finding quick and dirty solutions to problems. Märta Lewander Xu – thank you for always having the guts to say what you think. You have really helped me and guided me in many situations, including after finishing your Ph.D. Zuguang Guan – you were the person I came closest to at the beginning of my time at Atomic Physics, and you taught me a great deal. I was new to everything and was frankly quite frightened by your skills. I later found out that you were exceptionally good already at Zheijiang University, and I was slightly calmed. Liang Mei – you were my closest colleague toward the end of the thesis work. I believe we had great discussions and similar thoughts about physics. Thank you for always being prepared to help me out with all sorts of things. Lorenzo Cocola – you came as a guest PhD student from Italy to learn about our techniques. I am sure that you taught me more than I taught you. My visit to your temporary place in Höör with Anna was wonderful. Can Xu is always prepared to help me

out and to talk about other things than physics. Hiran Jayaweera – your positive spirit was great to be close to. I even got your bike when you left – this was the fastest bike I have ever had!

It has been great fun to work with all my coauthors from different disciplines. This type of cooperation is very important and I have learnt a lot from you. Some of these researchers I am grateful to are Emilie Krite Svanberg, Ursula Tylewicz, Anna Runemark, Susanne Åkesson, Annika Olsson, Vineta Fellman, Federico Gómez Galindo, Maren Wellenreuther, Erik Swietlicki, all our Italian TRS colleagues, and all the others I cannot provide room for here.

I also want to thank all the Masters and Bachelor students of the AMSRS group I met for understanding when I could not help you as much as I would like to: Marcus, Jan, Jim, Per, Jens, Tom, Anna-Lena, Anders, ...

All the people in the division deserve thanks for creating such a good working environment. Claes-Göran Wahlström deserves deep gratitude for his hard work to keep the division together. I would like to thank Anne, Camilla, Minna and Harriet for always being prepared to help us confused Ph.D. students (and not to talk about the professors).

A group of people (while I don't know who they are) deserve special thanks. These are all the referees of our published papers. This job is essential! Specifically, I am so grateful to one of the referees of Paper **XV**. Your document with suggestions for improvements was as long as the manuscript itself and improved it a great deal.

I want to thank the people who helped me with the photos on the front and back covers of the thesis – Nina, Therese, Stefan, David, Hugo, Mikkel, Anna and Haiyan.

Finally, I would like to acknowledge my appreciation to my family and old friends who gave me the best start in life and who are still there for me – always.

I want to thank my new family – Anna for coming into my life, for having a very similar and very different view on life, for your interest in nature, our environment and other big questions, and for sharing my temporary, crazy ideas to move to the country-side to grow vegetables. My son, Teodor, for preventing me from staying on my butt for too long, for being so happy, for showing me how much I actually owe my family, and for bringing new perspectives into life.

References

1. *Preparing for our future: Developing a common strategy for key enabling technologies in the EU*, vol. SEC2009 (The Commission of the European Communities, 2009).

2. M. Andersson, R. Grönlund, L. Persson, M. Sjöholm, K. Svanberg, and S. Svanberg, "Laser spectroscopy of gas in scattering media at scales ranging from kilometers to millimeters," *Laser Physics* 17, 893–902 (2007).

3. Y. J. Kim, U. Platt, M. B. Gu, and H. Iwahashi, *Atmospheric and biological environmental monitoring* (Springer, Heidelberg, 2009).

4. J. Artiola, I. Pepper, and M. Brusseau, *Environmental monitoring and characterization* (Elsevier, San Diego, 2004).

5. M. O. Andreae, "Soot carbon and excess fine potassium - long-range transport of combustion-derived aerosols," *Science* 220, 1148–1151 (1983).

6. M. O. Andreae, T. W. Andreae, R. J. Ferek, and H. Raemdonck, "Long-range transport of soot carbon in the marine atmosphere," *Science of the Total Environment* 36, 73–80 (1984).

7. S. E. Schwartz, *Trace atmospheric constituents: Properties, transformations, and fates* (Wiley, New York, 1983).

8. J. G. Calvert, *SO_2, NO and NO_2 oxidation mechanisms: atmospheric considerations* (Butterworth Publishers, Oxford, 1984).

9. *Health aspects of air pollusion with particulate matter, ozone and nitrogen dioxide* (World Health Organization, Bonn, 2003).

10. W. H. Schroeder and J. Munthe, "Atmospheric mercury – an overview," *Atmospheric Environment* 32, 809–822 (1998).

11. M. Vrekoussis, F. Wittrock, A. Richter, and J. P. Burrows, "Temporal and spatial variability of glyoxal as observed from space," *Atmospheric Chemistry and Physics* 9, 4485–4504 (2009).

12. S. Myriokefalitakis, M. Vrekoussis, K. Tsigaridis, F. Wittrock, A. Richter, C. Bruhl, R. Volkamer, J. P. Burrows, and M. Kanakidou, "The influence of natural and anthropogenic secondary sources on the glyoxal global distribution," *Atmospheric Chemistry and Physics* 8, 4965–4981 (2008).

13. M. Mullan and D. McDowell, *Modified atmosphere packaging*, pp. 263–294 (Wiley, Oxford, 2011), eds R. Coles, and M. Kirwan.

14. C. A. Phillips, "Review: Modified atmosphere packaging and its effects on the microbiological quality and safety of produce," *International Journal of Food Science & Technology* 31, 463–479 (1996).

15. A. R. Davies, *Advances in modified-atmosphere packaging*, chap. 14, pp. 304–320 (Springer, Philadelphia, 1995), ed. G. W. Gould.

16. I. Linnerud, P. Kaspersen, and T. Jaeger, "Gas monitoring in the process industry using diode laser spectroscopy," *Applied Physics B* 67, 297–305 (1998).

17. R. Hickling, D. B. Roy, J. K. Hill, and C. D. Thomas, "A northward shift of range margins in British Odonata," *Global Change Biology* 11, 502–506 (2005).

18. M. Campero, F. Ollevier, and R. Stoks, "Ecological relevance and sensitivity depending on the exposure time for two biomarkers," *Environmental Toxicology* 22, 572–81 (2007).

19. I. Newton, *The migration ecology of birds* (Academic Press, London, 2008).

20. T. Alerstam and A. Lindström, *Optimal bird migration: The relative importance of time, energy, and safety*, chap. 22, pp. 331–351 (Springer, Berlin, Heidelberg, 1990), ed. E. Gwinner.

21. T. Alerstam, A. Hedenström, and S. Åkesson, "Long-distance migration: evolution and determinants," *Oikos* 103, 247–260 (2003).

22. S. Zehnder, S. , F. Liechti, and B. Bruderer, "Nocturnal autumn bird migration at Falsterbo, South Sweden," *Journal of Avian Biology* 32, 239–248 (2001).

23. P. Kerlinger and F. Moore, *Atmospheric structure and avian migration*, vol. 6 of *Current Ornithology*, chap. 3, pp. 109–142 (Springer, Philadelphia, 1989), ed. D. M. Power.

24. A. Lindström, "The role of predation risk in stopover habitat selection in migrating bramblings, *Fringilla montifringilla*," *Behavioral Ecology* 1, 102–106 (1990).

25. B. Bruderer, "The study of bird migration by radar part 2: Major achievements," *Naturwissenschaften* 84, 45–54 (1997).

26. W. M. Gilbert, T. S. Nesbitt, and B. Danielsen, "The cost of prematurity: quantification by gestational age and birth weight," *Obstetrics & Gynecology* 102, 488–492 (2003).

27. A. Greenough, A. D. Milner, and G. Dimitriou, "Synchronized mechanical ventilation for respiratory support in newborn infants (Cochrane Review)," *Cochrane Database of Systematic Reviews* 2001 (2001).

28. L. B. Ware and M. A. Matthay, "Medical progress – the acute respiratory distress syndrome," *New England Journal of Medicine* 342, 1334–1349 (2000).

29. P. Panigrahi, "Necrotizing enterocolitis: A practical guide to its prevention and management," *Pediatric Drugs* 8, 151–165 (2006).

30. A. M. Kosloske, "Epidemiology of necrotizing enterocolitis," *Acta Paediatrica Supplement* 396, 2–7 (1994).

31. R. M. Kliegman and A. A. Fanaroff, "Nectrotizing enterocolitis," *New England Journal of Medicine* 310, 1093–1103 (1984).

32. J. Pietz, B. Achanti, L. Lilien, E. Clifford Stepka, and S. Ken Mehta, "Prevention of necrotitizing enterocolitis in preterm infants: a 20-year experience," *Pediatrics* 119, 164–170 (2006).

33. C. N. Banwell and E. M. McCash, *Fundamentals of molecular spectroscopy* (McGraw-Hill, Berkshire, 1994), 4 ed.

34. `http://en.wikipedia.org/wiki/Fraunhofer_lines`, retrieved 2014-02-12.

35. J. Buldyreva, N. Lavrentieva, and V. Starikov, *Collisional line broadening and shifting of atmospheric gases* (Imperial College Press, London, 2011).

36. W. Demtröder, *Laser spectroscopy: Basic principles*, vol. 1 (Springer, Berlin, Heidelberg, 2008), 4 ed.

37. C. Zender, "Radiative transfer in the earth system," (2010), `http://dust.ess.uci.edu/facts/rt/rt.pdf`, retrieved 2014-01-17.

38. J. Cooper, "Broadening of isolated lines in the impact approximation using a density matrix formulation," *Reviews of Modern Physics* 39, 167–177 (1967).

39. H. Margenau, "Pressure shift and broadening of spectral lines," *Physical Review* 40, 387–408 (1932).

40. A. Valentin, C. Claveau, A. D. Bykov, N. N. Lavrentieva, V. N. Saveliev, and L. N. Sinitsa, "The water-vapor ν_2 band lineshift coefficients induced by nitrogen pressure," *Journal of Molecular Spectroscopy* 198, 218–229 (1999).

41. N. Lavrentieva and A. Solodov, "Water vapor line shifts in the range 5000-5600 cm^{-1}; induced by the pressure of different buffer gases," *Optics and Spectroscopy* 98, 830–837 (2005).

42. T. M. Petrova, A. M. Solodov, and A. A. Solodov, "Measurements of water vapor line shifts in the 8650-9020 cm^{-1} region caused by pressure of atmospheric gases," *Atmospheric and Oceanic Optics* 23, 455–461 (2010).

43. L. R. Brown and C. Plymate, "Experimental line parameters of the oxygen A band at 760 nm," *Journal of Molecular Spectroscopy* 199, 166–179 (2000).

44. M. Lewander, *Laser absorption spectroscopy of gas in scattering media*, Ph.D. thesis, Lund University, Lund Reports on Atomic Physics, LRAP 424 (2010).

45. G. T. Fraser and S. L. Coy, "Absorber speed dependence of the coherence relaxation rate of the J = 0 - 1 transition of N_2O," *Journal of Chemical Physics* 83, 5687–5689 (1985).

46. L. Nguyen, J. Buldyreva, J. M. Colmont, F. Rohart, G. Wlodarczak, and E. A. Alekseev, "Detailed profile analysis of millimetre 502 and 602 GHz N_2O-$N_2(O_2)$ lines at room temperature for collisional linewidth determination," *Molecular Physics* 104, 2701–2710 (2006).

47. R. A. Toth, L. R. Brown, and C. Plymate, "Self-broadened widths and frequency shifts of water vapor lines between 590 and 2400 cm^{-1}," *Journal of Quantitative Spectroscopy Radiative Transfer* 59, 529–562 (1998).

48. M. Lepère, A. Henry, A. Valentin, and C. Camy-Peyret, "Diode-laser spectroscopy: Line profiles of H_2O in the region of 1.39 μm," *Journal of Molecular Spectroscopy* 208, 25–31 (2001).

49. R. H. Dicke, "The effect of collisions upon the Doppler width of spectral lines," *Physical Review* 89, 472–473 (1953).

50. L. Galatry, "Simultaneous effect of Doppler and foreign gas broadening on spectral lines," *Physical Review* 122, 1218–& (1961).

51. S. Rautian and I. Sobelman, "Influence on collisions on Doppler's width of spectral lines," *Soviet Physics Uspekhi-Ussr* 90, 209–236 (1966).

52. G. G. Stokes, "On the change of refrangibility of light," *Philosophical Transactions of the Royal Society of London* 142, 463–562 (1852).

53. S. Svanberg, *Atomic and molecular spectroscopy – Basic aspects and practical applications* (Springer, Berlin, Heidelberg, 2004), 4 ed.

54. F. Auzel, "Upconversion and anti-Stokes processes with f and d ions in solids," *Chemical Reviews* 104, 139–73 (2004).

55. C. T. Xu, Q. Q. Zhan, H. C. Liu, G. Somesfalean, J. Qian, S. L. He, and S. Andersson-Engels, "Upconverting nanoparticles for pre-clinical diffuse optical imaging, microscopy and sensing: current trends and future challenges," *Laser & Photonics Reviews* 7, 663–697 (2013).

56. K. Huang, W. K. Li, M. K. G. Jayakumar, and Y. Zhang, "Upconverting fluorescent nanoparticles for biodetection and photoactivation," *Advances in Photonics of Quantum Computing, Memory, and Communication VI* 8635 (2013).

57. H. C. Liu, C. T. Xu, G. Dumlupinar, O. B. Jensen, P. E. Andersen, and S. Andersson-Engels, "Deep tissue optical imaging of upconverting nanoparticles enabled by exploiting higher intrinsic quantum yield through use of millisecond single pulse excitation with high peak power," *Nanoscale* 5, 10034–10040 (2013).

58. M. Lackner, "Tunable diode laser absorption spectroscopy (TDLAS) in the process industries – a review," *Reviews in Chemical Engineering* 23, 65 (2007).

59. M. W. Sigrist, R. Bartlome, D. Marinov, J. M. Rey, D. E. Vogler, and H. Wächter, "Trace gas monitoring with infrared laser-based detection schemes," *Applied Physics B* 90, 289–300 (2008).

60. K. Song and E. C. Jung, "Recent developments in modulation spectroscopy for trace gas detection using tunable diode lasers," *Applied Spectroscopy Reviews* 38, 395–432 (2003).

61. M. Andersson, *Development of laser spectroscopy for scattering media applications*, Ph.D. thesis, Lund University, Lund Reports on Atomic Physics, LRAP 383 (2007).

62. L. Persson, *Laser spectroscopy in scattering media for biological and medical applications*, Ph.D. thesis, Lund University, Lund Reports on Atomic Physics, LRAP 385 (2007).

63. M. Brydegaard, *Aspects of optical broad band spectroscopy and information extraction*, Ph.D. thesis, Lund University, Lund Reports on Atomic Physics, LRAP 462 (2012).

64. L. Mei, *Light propagation and gas absorption studies in turbid media using tunable diode laser techniques*, Ph.D. thesis, Lund University, Lund Reports on Atomic Physics, LRAP 486 (2014).

65. A. Beer, "Bestimmung der Absorption des rothen Lichts in farbigen Flüssigkeiten," *Annalen der Physik* 162, 78–88 (1852).

66. O. Axner, J. Gustafsson, F. M. Schmidt, N. Omenetto, and J. D. Winefordner, "A discussion about the significance of absorbance and sample optical thickness in conventional absorption spectrometry and wavelength-modulated laser absorption spectrometry," *Spectrochimica Acta Part B: Atomic Spectroscopy* 58, 1997–2014 (2003).

67. P. Werle, "A review of recent advances in semiconductor laser based gas monitors," *Spectrochimica Acta Part A: Molecular and Biomolecular Spectroscopy* 54, 197–236 (1998).

68. E. I. Moses and C. L. Tang, "High-sensitivity laser wavelength-modulation spectroscopy," *Optics Letters* 1, 115–117 (1977).

69. P. Kluczynski, J. Gustafsson, A. M. Lindberg, and O. Axner, "Wavelength modulation absorption spectrometry – an extensive scrutiny of the generation of signals," *Spectrochimica Acta Part B – Atomic Spectroscopy* 56, 1277–1354 (2001).

70. G. C. Björklund, "Frequency-modulation spectroscopy - new method for measuring weak absorptions and dispersions," *Optics Letters* 5, 15–17 (1980).

71. D. S. Bomse, A. C. Stanton, and J. A. Silver, "Frequency-modulation and wavelength modulation spectroscopies - comparison of experimental methods using a lead-salt diode-laser," *Applied Optics* 31, 718–731 (1992).

72. J. A. Silver, "Frequency-modulation spectroscopy for trace species detection - theory and comparison among experimental methods," *Applied Optics* 31, 707–717 (1992).

73. P. Kluczynski and O. Axner, "Theoretical description based on Fourier analysis of wavelength-modulation spectrometry in terms of analytical and background signals," *Applied Optics* 38, 5803–5815 (1999).

74. J. Reid and D. Labrie, "Second-harmonic detection with tunable diode lasers – comparison of experiment and theory," *Applied Physics B* 26, 203–210 (1981).

75. T. Fernholz, H. Teichert, and V. Ebert, "Digital, phase-sensitive detection for *in situ* diode-laser spectroscopy under rapidly changing transmission conditions," *Applied Physics B* 75, 229–236 (2002).

76. M. Andersson, L. Persson, T. Svensson, and S. Svanberg, "Flexible lock-in detection system based on synchronized computer plug-in boards applied in sensitive gas spectroscopy," *Review of Scientific Instruments* 78, 113107 (2007).

77. L. Persson, M. Lewander, M. Andersson, K. Svanberg, and S. Svanberg, "Simultaneous detection of molecular oxygen and water vapor in the tissue optical window using tunable diode laser spectroscopy," *Applied Optics* 47, 2028–2034 (2008).

78. T. Svensson, *Pharmaceutical and biomedical applications of spectroscopy in the photom migration regime*, Ph.D. thesis, Lund University, Lund Reports on Atomic Physics, LRAP 392 (2008).

79. M. Lewander, Z. Guan, K. Svanberg, S. Svanberg, and T. Svensson, "Clinical system for non-invasive in situ monitoring of gases in the human paranasal sinuses," *Optics Express* 17, 10849–10863 (2009).

80. J. S. Belrose, "Reginald Aubrey Fessenden and the birth of wireless telephony," *IEEE Antennas and Propagation Magazine* 44, 38–47 (2002).

81. J. Marszal and R. Salamon, "Distance measurement errors in silent FM-CW sonar with matched filtering," *Metrology and Measurement Systems* 19, 321–332 (2012).

82. L. Kay, "A comparison between pulse and frequency-modulation echo-ranging systems," (1959).

83. A. G. Stove, "Linear FMCW radar techniques," *IEEE Proceedings – F Radar and Signal Processing* 139, 343–350 (1992).

84. D. Uttam and B. Culshaw, "Precision time domain reflectometry in optical fiber systems using a frequency modulated continuous wave ranging technique," *Lightwave Technology, Journal of* 3, 971–977 (1985).

85. S. Svanberg, "Lidar," pp. 1031–1052, Springer Handbook of Lasers and Optics (Springer, Heidelberg, 2007).

86. R. M. Measures, *Laser remote sensing: fundamentals and applications* (Wiley, New York, 1984).

87. J. Zheng, *Optical Frequency-Modulated Continuous-Wave (FMCW) Interferometry* (Springer, New York, 2005).

88. O. Batet, F. Dios, and A. Comeron, "FMCW lidar for multiple-target sounding," in "SPIE Proceedings," , vol. 7813, pp. 78130H–1–78130H–11.

89. N. Takeuchi, *Elastic lidar measurements of the troposphere*, pp. 63–122 (CRC Press, Boca Raton, 2005), eds T. Fujii, and T. Fukuchi.

90. P. Weibring, J. N. Smith, H. Edner, and S. Svanberg, "Development and testing of a frequency-agile optical parametric oscillator system for differential absorption lidar," *Review of Scientific Instruments* 74, 4478–4484 (2003).

91. S. Svanberg, *Fluorescence spectroscopy and imaging of LIDAR targets*, pp. 433–468 (CRC press, Boca Raton, 2005), eds T. Fujii, and T. Fukuchi.

92. X. Chu and G. C. Papen, *Resonance fluorescence lidar*, pp. 63–122 (CRC Academic Press, Boca Raton, 2005), eds T. Fujii, and T. Fukuchi.

93. K. S. Arnold and C. Y. She, "Metal fluorescence lidar (light detection and ranging) and the middle atmosphere," *Contemporary Physics* 44, 35–49 (2003).

94. R. A. O'Neil, L. Bujabijunas, and D. M. Rayner, "Field performance of a laser fluorosensor for the detection of oil spills," *Applied Optics* 19, 863–870 (1980).

95. J. Vasilescu, L. Marmureanu, E. Carstea, and C. P. Cristescu, "Oil spills detection from fluorescence lidar measurements," *University Politehnica of Bucharest Scientific Bulletin – Series A – Applied Mathematics and Physics* 72, 149–154 (2010).

96. R. Barbini, F. Colao, R. Fantoni, A. Palucci, and S. Ribezzo, "Lidar monitoring of dinoflagellate algal bloom on the Swedish coast," *Remote Sensing of Vegetation and Water, and Standardization of Remote Sensing Methods* 3107, 217–228 (1997).

97. G. Cecchi and L. Pantani, "Vegetation monitoring by means of spectral resolved fluorescence lidar," *Physical Measurements and Signatures in Remote Sensing* 319, 687–689 (1991).

98. H. Edner, J. Johansson, S. Svanberg, and E. Wallinder, "Fluorescence lidar multicolor imaging of vegetation," *Applied Optics* 33, 2471–2479 (1994).

99. S. Svanberg, "Fluorescence lidar monitoring of vegetation status," *Physica Scripta* T58, 79–85 (1995).

100. L. Pantani, G. Ballerini, G. Cecchi, H. Edner, D. Lognoli, T. Johansson, V. Raimondi, S. Svanberg, P. Tiano, L. Tomaselli, and P. Weibring, "Experiments on stony monument monitoring by laser-induced fluorescence," *Journal of Cultural Heritage* 1, S345–S348 (2000).

101. V. Raimondi, G. Cecchi, L. Pantani, and R. Chiari, "Fluorescence lidar monitoring of historic buildings," *Applied Optics* 37, 1089–1098 (1998).

102. P. Weibring, T. Johansson, H. Edner, S. Svanberg, B. Sundnér, V. Raimondi, G. Cecchi, and L. Pantani, "Fluorescence lidar imaging of historical monuments," *Applied Optics* 40, 6111–6120 (2001).

103. J. Hällström, K. Barup, R. Grönlund, A. Johansson, S. Svanberg, L. Palombi, D. Lognoli, V. Raimondi, G. Cecchi, and C. Conti, "Documentation of soiled and biodeteriorated facades: A case study on the Coliseum, Rome, using hyperspectral imaging fluorescence lidars," *Journal of Cultural Heritage* 10, 106–115 (2009).

104. L. Palombi, D. Lognoli, V. Raimondi, G. Cecchi, J. Hällstrom, K. Barup, C. Conti, R. Grönlund, A. Johansson, and S. Svanberg, "Hyperspectral fluorescence lidar imaging at the colosseum, rome: Elucidating past conservation interventions," *Optics Express* 16, 6794–6808 (2008).

105. M. Sjöholm, G. Somesfalean, J. Alnis, S. Andersson-Engels, and S. Svanberg, "Analysis of gas dispersed in scattering media," *Optics Letters* 26, 16–18 (2001).

106. S. Svanberg, "Optical analysis of trapped gas gas in scattering media absorption spectroscopy," *Laser Physics* 20, 68–77 (2010).

107. S. Svanberg, "Gas in scattering media absorption spectroscopy – from basic studies to biomedical applications," *Laser & Photonics Reviews* 7, 779–796 (2013).

108. G. M. Hale and M. R. Querry, "Optical constants of water in the 200-nm to 200-μm wavelength region," *Applied Optics* 12, 555–563 (1973).

109. S. Prahl, "Tabulated molar extinction coefficient for hemoglobin in water," (1998), `http://omlc.ogi.edu/spectra/hemoglobin/summary.html`, retrieved 2013-11-18.

110. L. Mei, G. Somesfalean, and S. Svanberg, "Pathlength determination for gas in scattering media absorption spectroscopy," *Sensors* 14, 3871–3890 (2014).

111. M. Lewander, Z. Guan, L. Persson, A. Olsson, and S. Svanberg, "Food monitoring based on diode laser gas spectroscopy," *Applied Physics B* 93, 619–625 (2008).

112. L. Persson, M. Andersson, M. Cassel-Engquist, K. Svanberg, and S. Svanberg, "Gas monitoring in human sinuses using tunable diode laser spectroscopy," *Journal of Biomedical Optics* 12, 2028–2034 (2007).

113. L. Persson, H. Gao, M. Sjöholm, and S. Svanberg, "Diode laser absorption spectroscopy for studies of gas exchange in fruits," *Optics and Lasers in Engineering* 44, 687–698 (2006).

114. M. Andersson, L. Persson, M. Sjöholm, and S. Svanberg, "Spectroscopic studies of wood-drying processes," *Optics Express* 14, 3641–3653 (2006).

115. J. Johansson, S. Folestad, M. Josefson, A. Sparén, C. Abrahamsson, S. Andersson-Engels, and S. Svanberg, "Time-resolved NIR/Vis spectroscopy for analysis of solids: Pharmaceutical tablets," *Applied Spectroscopy* 56, 725–731 (2002).

116. W. F. Long and D. H. Burns, "Particle sizing and optical constant measurement in granular samples using statistical descriptors of photon time-of-flight distributions," *Analytica Chimica Acta* 434, 113–123 (2001).

117. B. Chance, J. S. Leigh, H. Miyake, D. S. Smith, S. Nioka, R. Greenfeld, M. Finander, K. Kaufmann, W. Levy, and M. Young, "Comparison of time-resolved and -unresolved measurements of deoxyhemoglobin in brain," *Proceedings of*

the National Academy of Sciences of the United States of America **85**, 4971–5 (1988).

118. A. P. Gibson, J. C. Hebden, and S. R. Arridge, "Recent advances in diffuse optical imaging," *Physics in Medicine and Biology* **50**, R1–43 (2005).

119. R. Berg, O. Jarlman, and S. Svanberg, "Medical transillumination imaging using short-pulse diode-lasers," *Applied Optics* **32**, 574–579 (1993).

120. J. C. Hebden and H. Rinneberg, *Special section on time-domain optical mammography* (Institute of Physics Pub., Bristol, 2005).

121. P. Taroni, D. Comelli, A. Pifferi, A. Torricelli, and R. Cubeddu, "Absorption of collagen: effects on the estimate of breast composition and related diagnostic implications," *Journal of Biomedical Optics* **12**, 014021 (2007).

122. T. Svensson, S. Andersson-Engels, M. Einarsdottir, and K. Svanberg, "*In vivo* optical characterization of human prostate tissue using near-infrared time-resolved spectroscopy," *Journal of Biomedical Optics* **12**, 014022–014022 (2007).

123. J. R. Lorenzo, *Principles of diffuse light propagation: Light propagation in tissues with applications in biology and medicine* (World Scientific Publishing, Singapore, 2012).

124. D. V. O'Connor and D. Phillips, *Time-correlated single photon counting* (Academic Press, London, 1984).

125. G. Somesfalean, M. Sjöholm, J. Alnis, C. af Klinteberg, S. Andersson-Engels, and S. Svanberg, "Concentration measurement of gas embedded in scattering media by employing absorption and time-resolved laser spectroscopy," *Applied Optics* **41**, 3538–3544 (2002).

126. B. Chance, M. Cope, E. Gratton, N. Ramanujam, and B. Tromberg, "Phase measurement of light absorption and scatter in human tissue," *Review of Scientific Instruments* **69**, 3457–3481 (1998).

127. L. Mei, S. Svanberg, and G. Somesfalean, "Combined optical porosimetry and gas absorption spectroscopy in gas-filled porous media using diode-laser-based frequency domain photon migration," *Optics Express* **20**, 16942–16954 (2012).

128. L. Mei, S. Svanberg, and G. Somesfalean, "Frequency-modulated light scattering in colloidal suspensions," *Applied Physics Letters* **102**, 061104–1–061104–4 (2013).

129. L. Mei, G. Somesfalean, and S. Svanberg, "Frequency-modulated light scattering interferometry used for assessment of optical properties in turbid media," in "SPIE Proceedings," , vol. 8579, pp. 85790O–85790O–7.

130. A. L. Buck, "New equations for computing vapor-pressure and enhancement factor," *Journal of Applied Meteorology* 20, 1527–1532 (1981).

131. T. Svensson and Z. Shen, "Laser spectroscopy of gas confined in nanoporous materials," *Applied Physics Letters* 96, 021107 (2010).

132. T. Svensson, M. Lewander, and S. Svanberg, "Laser absorption spectroscopy of water vapor confined in nanoporous alumina: wall collision line broadening and gas diffusion dynamics," *Optics Express* 18, 16460–73 (2010).

133. C. T. Xu, M. Lewander, S. Andersson-Engels, E. Adolfsson, T. Svensson, and S. Svanberg, "Wall-collision line broadening of molecular oxygen within nanoporous materials," *Physical Review A* 84, 042705 (2011).

134. T. Svensson, E. Adolfsson, M. Burresi, R. Savo, C. T. Xu, D. S. Wiersma, and S. Svanberg, "Pore size assessment based on wall collision broadening of spectral lines of confined gas: experiments on strongly scattering nanoporous ceramics with fine-tuned pore sizes," *Applied Physics B* 110, 147–154 (2013).

135. J. M. Hartmann, V. Sironneau, C. Boulet, T. Svensson, J. T. Hodges, and C. T. Xu, "Collisional broadening and spectral shapes of absorption lines of free and nanopore-confined O_2 gas," *Physical Review A* 87, 032510 (2013).

136. L. Eriksson, E. Johansson, N. Kettaneh-Wold, J.Trygg, C. Wikström, and S. Wold, *Multi- and megavariate data analysis, part I* (Umetrics AB, Umeå, 2006).

137. K. R. Beebe and B. R. Kowalski, "An introduction to multivariate calibration and analysis," *Analytical Chemistry* 59, 1007A–1017A (1987).

138. L. Persson, F. Andersson, M. Andersson, and S. Svanberg, "Approach to optical interference fringes reduction in diode laser absorption spectroscopy," *Applied Physics B – Lasers and Optics* 87, 523–530 (2007).

139. J. A. Silver and A. C. Slanton, "Optical interference fringe reduction in laser absorption experiments," *Applied Optics* 27, 1914–1916 (1988).

140. D. Masiyano, J. Hodgkinson, S. Schilt, and R. P. Tatam, "Self-mixing interference effects in tunable diode laser absorption spectroscopy," *Applied Physics B* 96, 863–874 (2009).

141. P. Vogel and V. Ebert, "Near shot noise detection of oxygen in the A-band with vertical-cavity surface-emitting lasers," *Applied Physics B* 72, 127–135 (2001).

142. J. Alnis, B. Anderson, M. Sjöholm, G. Somesfalean, and S. Svanberg, "Laser spectroscopy of free molecular oxygen dispersed in wood materials," *Applied Physics B* 77, 691–695 (2003).

143. L. Persson, K. Svanberg, and S. Svanberg, "On the potential of human sinus cavity diagnostics using diode laser gas spectroscopy," *Applied Physics B* 82, 313–317 (2006).

144. M. Lewander, S. Lindberg, T. Svensson, R. Siemund, K. Svanberg, and S. Svanberg, "Non-invasive diagnostics of the maxillary and frontal sinuses based on diode laser gas spectroscopy," *Rhinology* 50, 26–32 (2012).

145. M. Lewander, A. Bruzelius, S. Svanberg, K. Svanberg, and V. Fellman, "Non-intrusive gas monitoring in neonatal lungs using diode laser spectroscopy: feasibility study," *Journal of Biomedical Optics* 16, 127002 (2011).

146. T. Svensson, L. Persson, M. Andersson, S. Svanberg, S. Andersson-Engels, J. Johansson, and S. Folestad, "Non-invasive characterization of pharmaceutical solids by diode laser oxygen spectroscopy," *Applied Spectroscopy* 61, 784–786 (2007).

147. T. Svensson, M. Andersson, L. Rippe, S. Svanberg, S. Andersson-Engels, J. Johansson, and S. Folestad, "VCSEL-based oxygen spectroscopy for structural analysis of pharmaceutical solids," *Applied Physics B* 90, 345–354 (2008).

148. T. Svensson, E. Adolfsson, M. Lewander, C. T. Xu, and S. Svanberg, "Disordered, strongly scattering porous materials as miniature multipass gas cells," *Physical Review Letters* 107, 143901 (2011).

149. J. Shaw, N. Seldomridge, D. Dunkle, P. Nugent, L. Spangler, J. Bromenshenk, C. Henderson, J. Churnside, and J. Wilson, "Polarization lidar measurements of honey bees in flight for locating land mines," *Optics Express* 13, 5853–63 (2005).

150. K. S. Repasky, J. A. Shaw, R. Scheppele, C. Melton, J. L. Carsten, and L. H. Spangler, "Optical detection of honeybees

by use of wing-beat modulation of scattered laser light for locating explosives and land mines," *Applied Optics* 45, 1839–1843 (2006).

151. D. S. Hoffman, A. R. Nehrir, K. S. Repasky, J. A. Shaw, and J. L. Carlsten, "Range-resolved optical detection of honey-bees by use of wing-beat modulation of scattered light for locating land mines," *Applied Optics* 46, 3007–12 (2007).

152. R. O. Prum, J. A. Cole, and R. H. Torres, "Blue integumentary structural colours in dragonflies (*Odonata*) are not produced by incoherent Tyndall scattering," *The Journal of Experimental Biology* 207, 3999–4009 (2004).

153. M. Brydegaard, Z. Guan, M. Wellenreuther, and S. Svanberg, "Insect monitoring with fluorescence lidar techniques: feasibility study," *Applied Optics* 48, 5668–5677 (2009).